



City Research Online

City, University of London Institutional Repository

Citation: Qian, K., Lan, X., Li, Z. & Fu, F. (2021). Behavior of Steel Moment Frames using Top-and-Seat Angle Connections under Various Column Removal Scenarios. *Journal of Structural Engineering*, 147(10), 04021144. doi: 10.1061/(ASCE)ST.1943-541X.0003089

This is the accepted version of the paper.

This version of the publication may differ from the final published version.

Permanent repository link: <https://openaccess.city.ac.uk/id/eprint/25873/>

Link to published version: [https://doi.org/10.1061/\(ASCE\)ST.1943-541X.0003089](https://doi.org/10.1061/(ASCE)ST.1943-541X.0003089)

Copyright: City Research Online aims to make research outputs of City, University of London available to a wider audience. Copyright and Moral Rights remain with the author(s) and/or copyright holders. URLs from City Research Online may be freely distributed and linked to.

Reuse: Copies of full items can be used for personal research or study, educational, or not-for-profit purposes without prior permission or charge. Provided that the authors, title and full bibliographic details are credited, a hyperlink and/or URL is given for the original metadata page and the content is not changed in any way.

Behavior of Steel Moment Frames using Top-and-Seat Angle Connections under Various Column Removal Scenarios

Kai Qian¹ Ph.D, M.ASCE, Xi Lan², Zhi Li³ and Feng Fu⁴, C.Eng, F.ASCE

ABSTRACT

Top-and-seat angle connection is a conventional type of steel moment connection. However, its capacity in accommodating columns loss is rarely studied. In this study, five multi-story steel moment sub-frames using top-and-seat angle connection were fabricated and tested to investigate their performance subjected to various column removal scenarios including: (a) a middle column loss; (b) a penultimate column loss; and (c) a corner column loss. Moreover, the effects of the thickness of steel angle on load resistance were quantified. The test results indicated that load resisting capacity increased significantly with the increase of angle thickness. In both middle column and penultimate column removal scenarios, catenary action was developed in the frames. It is also noticed that, flexural action dominated the load resisting mechanism of the frames under a corner column loss scenario. For beams in different stories, similar flexural resistance was developed. However, the beams in the first story are able to develop larger catenary action than that in the second story. It worth noting that, for a corner column missing scenario, Vierendeel action helps to enhance the flexural action significantly.

CE Database subject heading: experimental; analytical; progressive collapse; steel; moment frame

¹ Professor in College of Civil Engineering and Architecture at Guilin University of Technology, China, 541004, (corresponding author) qiankai@glut.edu.cn

² Research Student in College of Civil Engineering and Architecture at Guangxi University, China, 530004, lanx@st.gxu.edu.cn

³ Research Fellow in College of Civil Engineering and Architecture at Guilin University of Technology, China, 531004, lizhi@st.gxu.edu.cn

⁴ Senior Lecturer in Structural Engineering, School of Mathematics, Computer Science and Engineering, City, University of London, U.K., Feng.Fu.1@city.ac.uk

30 INTRODUCTION

31 Progressive collapse is defined as the initial local failure leading to the disproportionate collapse
32 of the building. Although progressive collapse is a relatively low likelihood event, considerable loss of
33 live and properties were involved. Thus, deep understanding on its capacity to prevent progressive
34 collapse is essential. After the collapse of Ronan Point building, the alternative load path (ALP) method
35 was proposed as a main direct design method in design guidelines (DoD 2010 and GSA 2013) due to
36 its event independent merit.

37 In the past decade, relied on ALP method, extensive quasi-static tests were conducted to
38 evaluate the mechanism of steel frames to resist progressive collapse (Lee et al. 2010; Dinu et al. 2016;
39 Qin et al. 2016; Dinu et al. 2017; Tang et al. 2019; Wang et al. 2019; Gao et al. 2017; Qian et al. 2020a).
40 For welded connection, the fracture generally occurred at the beam flanges near the welds (Li et al.
41 2007; Li et al. 2017). The brittle fracture of weld leads to low deformation capacity, which is essential
42 to the development of catenary action (Li et al. 2018; Qian et al. 2020a). For seismically configured
43 steel frames, to increase the deformation capacity and ductility, reduced beam section (RBS) was
44 adopted for welded connection (Khandelwal and Ei-Tawil 2007; Sadek et al. 2011; Lew et al. 2013;
45 Wang et al. 2020). It was found that flexural action and catenary action were the primary load resisting
46 mechanisms for steel frames subjected to a middle column loss scenario (Alashker et al. 2011; Liu et
47 al. 2015; Meng et al. 2019; Zhong et al. 2020; Dimopoulos et al. 2020; Wang et al. 2016). Compressive
48 arch action was normally ignored in steel frames to resist progressive collapse due to relatively large
49 span-to-depth ratio. However, Lu et al. (2019) found that for composite frames, compressive arch
50 action was developed in steel beams, but the local buckling occurred on the compressive flange at beam
51 end, may reduce the efficiency of compressive arch action.

52 Compared to welded connections, the bolted angle connection, such as top-and-seat angle
53 connections, exhibits greater ductility and deformation capacity. The seismic behavior of top-and-seat
54 angle connections has been studied extensively (Shen and Astaneh-Asl 1999; Garlock et al. 2003;
55 Danesh et al. 2007; Gong 2014; Abdalla et al. 2015; Davaran et al. 2019; Beland et al. 2020a, b, c). It
56 was found that the angle thickness is one of the most critical parameters on the nonlinear behavior of

the connection (Azizinamini 1982; Garlock et al. 2003; Shen and Astanesh-Asl 1999; Abdalla et al. 2015). For connections with thin angles, plastic hinges were formed in the extruded leg of the angles. However, for relatively thick angles, the plastic hinge might form at the central line of the column bolts (Shen and Astanesh-Asl 1999). In addition, based on the deflection shape, a three-linear moment–rotation behavior was proposed by Shen and Astanesh-Asl (1999). Compared to seismic behavior of top-and-seat angle connection, investigations on their progressive collapse behavior are fewer (Yang and Tan 2013a, b; Oosterhof and Driver 2015; Weigand and Berman 2016; and Gong 2017). Yang and Tan (2013a, b) studied different types of steel frames with bolted angle connections under a middle column removal scenario. The behavior and failure modes of different connections are presented and discussed. Gong (2017) found that steel frames with top-and-seat angle connection developed both flexural action and compressive arch action in their tests. A compressive spring model was proposed for simulating progressive collapse behavior of the top-and-seat angle connection.

However, as proposed by DoD (2010) and previous studies (Stevens et al. 2011; Fu 2009,2010,2012), the building should be evaluated extensively under different column missing scenarios including: a) the loss of an interior column, b) the loss of a penultimate column, and c) the loss of a corner column, etc. This is because the development of load resisting mechanism depends on the position of column removal. Different boundary condition should be applied on the tested specimens in accordance with different column removal scenarios. Moreover, studies on steel frames subjected to the loss of a penultimate column or a corner column was rare. Furthermore, although progressive collapse behavior of a structure is a global response, majority of existing tests on steel frames against progressive collapse only relied on simplified single-story beam-column sub-assemblages, ignoring the interaction of structural components in different stories.

Therefore, in this study, five two-story by two-bay 1/2-scale steel sub-frames were fabricated and tested to investigate the load resisting mechanism of the steel frame using top-and-seat angle connections under different column missing scenarios. To deeply understand the load resisting mechanism of steel frames using this type of connections, analytical analysis was also made.

83 **EXPERIMENTAL PROGRAM**

84 **Test specimens**

85 As shown in Fig. 1, a six-story, 6×6 bay prototype steel moment frame with non-seismic design
86 configuration was fabricated in accordance with AISC-360 (2005). The designed dead and live loads
87 are 5.1 kN/m² and 3.0 kN/m², respectively. The story height of the prototype frame is 3.0 m with span
88 length of the frame in longitudinal and transverse direction was 8.4 m by 6.0 m, respectively.
89 Considering fabrication cost and facility capacity of the laboratory, only two-bay by two-story sub-
90 frame was extracted from the prototype frame and scaled down by a factor of 2.0. To simulate
91 horizontal restraints from the surrounding bays, beam was extended with length of 655 mm beyond the
92 side column, if any, as shown in Fig. 2a. As pointed out below, a horizontal roller was utilized to
93 connect the overhanging beam and A-frame.

94 The geometric details of top-and-seat angle connection are shown in Fig. 3. Although 1/2-scale
95 specimens were tested, the connection configurations, which were scaled down proportionally, were
96 still commonly used as in practice. Chinese section HN 200×100×5.5×8 (equivalent to American W
97 shape of W8×5^{1/4}×18 unit in in.) was used for beams whereas HW 150×150×7×10 (equivalent to
98 American W shape of W6×6×20 unit in in.) was for columns. Continuity plates with thickness of 10
99 mm were provided in the column. Steel angles with size of 70 mm×6 mm, 70 mm ×8 mm, and 70
100 mm×10 mm was used as top-and-seat angle to connect beam and column flanges. Grade 8.8 M18 bolt
101 were used with nut and washer. Bolts were preload of 345 N·m, which was applied by a torque wrench,
102 was adopted to bolt fastening. Specimen properties are listed in Table 1, in which TSC, TSP, and TSM
103 represent the specimens under a corner, a penultimate, and a middle column removal scenario,
104 respectively. It should be noted that the number 6, 8, and 10 represent the thickness of steel angle. For
105 example, TSP-8 represents steel sub-frame with top-and-seated angle connection, which was fabricated
106 by 8 mm thick steel angle, subjected to the loss of a penultimate column scenario.

107 **Material properties**

108 Chinese Q235 steel was used for column, beam, and angle. The measured yield strength, ultimate
109 strength, and elongation of the angle and structural components are tabulated in Table 2. As no

110 independent coupon test was conducted for bolts (Grade 8.8 M18), the yield stress and ultimate strength
111 of the bolts are the value provided by supplier.

112 **Test setup**

113 For TSM-8 and TSP-8, as shown in Figs. 4a and b, the bottom of each edge column was pin
114 supported. The beam overhang, if any, was connected to the A-frame via a roller connection. The
115 columns at ground story were removed at different location prior to applying concentrated load to
116 replicate initial local damage. The vertical load was applied by a hydraulic jack (Item 1 in Fig. 4a) at
117 the top of joints, where a column was removed in advance, by displacement-controlled loading method.
118 This method was relied on the merit of alternate load path method and had been adopted by extensive
119 previous studies (Lee et al. 2010; Sadek et al. 2013, Yang and Tan 2013a, b; Wang et al. 2017; Qian et
120 al. 2020a, b). However, it should be noted that the uniformly distributed live load and dead load were
121 ignored herein, which may change the failure mode and deformation capacity of the specimens (Qian
122 et al. 2020c). To prevent any undesired out-of-plane failure, a steel assembly (Item 3 in Fig. 4a) was
123 installed beneath the hydraulic jack (Item 1 in Fig. 4a). Side column was applied axial force with axial
124 compressive ratio of 0.3 via a hydraulic jack (Item 4 in Fig. 4a) to represent the loads from above floor.

125 Fig. 4c shows the test setup of TSC-8, which replicated the loss of a corner column. To allow
126 possible rotation of the corner column, a one-way hinge (Item 8 in Fig. 4c) was installed at the top of
127 the corner column. To prevent out-of-plane failure of the beams in ground story, a pair of supporting
128 beams (Item 9 in Fig. 4c) with rollers was installed. As shown in Fig. 2, the strain at critical sections
129 was monitored by a series of strain gauges or strain gauge rosettes. Thus, the axial forces and bending
130 moments of the beam sections could be determined by simplified section analysis.

131 **Instrumentations**

132 Instrumentations are shown in Fig. 4. A load cell (Item 2 in Fig. 4a) was installed below the
133 hydraulic jack (Item 1 in Fig. 4a) to measure the applied concentrated load. Tension/compression load
134 cell (Item 5 in Fig. 4a) was installed at each roller to measure its horizontal reaction force. A load pin
135 (Item 6 in Fig. 4a) was installed at each pin support to measure the horizontal reaction force of the

136 bottom pin support. In addition, a series of linear variable differential transformers (LVDTs) (Item 7
137 in Fig. 4a) were installed along the beam span in ground story, as shown in Fig. 4a.

138 **EXPERIMENTAL RESULTS**

139 **Vertical load and failure modes**

140 **TSC-8:** The key results are listed in Table 3. The measured load-displacement curves at the
141 joints of the lost column of TSC-8, TSP-8, and TSM-8 are compared in Fig. 5. For TSC-8, the yield
142 load (YL) of 5.1 kN was measured when the displacement at lost column (DLC) reached 40 mm.
143 Therefore, the initial stiffness, which is defined as the ratio of yield load to corresponding yield
144 displacement, of TSC-8 was 0.13 kN/mm. TSC-8 reached the peak load (PL) of 16.6 kN at a DLC of
145 310 mm. At this displacement stage, fracture occurred at a bottom angle close to the corner column in
146 the second story. Further increasing the displacement, the load resistance started to drop gradually. At
147 a DLC of 345 mm, the bottom angle near the corner column in the second story fractured completely.
148 Then, the top angle close to the corner column in the second story, which was initially suffered
149 compressive force, become in tension. When DLC reached 403 mm, the top angle near the side column
150 in the ground story fractured. However, the load resistance did not loss completely due to the
151 unfractured bottom angle. Further increasing the DLC, the bolted holes of the bottom angle at the
152 corner joint in the first ground were tore off. The bolted holes at the position of column leg of the top
153 angle at the side column in the second story deformed from circular to elliptical, which resulted in the
154 loss of load resistance significantly. The failure mode of TSC-8 is shown in Fig. 6. As shown in the
155 figure, fracture was observed at the bottom angle in Joint A and top angle in Joint B. Although no angle
156 fracture was observed in Joints C and D, the damage was concentrated in the bolted holes, either
157 achieved significant plastic deformation or tearing failure.

158 **TSP-8:** As shown in Fig. 5, the YL of 11.0 kN was measured at a DLC of 20 mm. Thus, the initial
159 stiffness was 0.55 kN/mm. The right and left bottom angle near the middle column in the ground story
160 fractured at a DLC of 302 mm and 324 mm, respectively. However, after sudden drop of the load
161 resistance due to the angle fracture, the load resistance kept increasing. When the DLC reached 500

162 mm, the increase of load resistance become gently as the top angle near the side column was yielded
163 at the center-line of the bolts. When the DLC reached 564 mm, the PL of 39.8 kN was recorded. After
164 that, the fracture of angle near the middle column in the second story occurred. The failure mode of
165 TSP-8 is shown in Fig. 7. As shown in the figure, the heel of bottom angle near the middle column
166 fractured at Joints A and B. However, as shown in Joints C and D, although fracture was also occurred
167 at the top angle close to the side column, the fracture of the angle occurred at the center-line of the
168 bolts, which actually performed more ductile.

169 **TSM-8 :** For TSM-8, the YL of 13.5 kN was measured at a DLC of 20 mm. The initial stiffness
170 of TSM-8 is 0.68 kN/mm, which is about 523.0 % and 123.6 % of that of TSC-8 and TSP-8,
171 respectively. The left and right angle near the middle column in the ground story fractured at the DLC
172 of 291 mm and 316 mm, respectively. Compared to TSP-8, the angle fractured earlier. The PL of 44.4
173 kN, which is 111.7 % of that of TSP-8, is measured at a DLC of 394 mm. At this stage, the bottom
174 angle at the left side of the middle column in the second story fractured. Then, the load resistance
175 dropped over 43.3 % due to the fracture of the bottom angle near the right side of middle column in
176 the second story. Further increasing DLC to 447 mm, 459 mm, and 487 mm, top angles near the side
177 columns were fractured in sequence. However, as shown in Fig. 8, if uniformly distributed dead load
178 and live load was simulated in the test setup, the failure may first occur at the beam end near the side
179 column due to slightly greater bending moment occurred there. Thus, ignoring the uniform distributed
180 live load and dead load may change the failure mode. The failure mode of TSM-8 is shown in Fig. 9.
181 In general, the failure mode of TSM-8 is similar to that of TSP-8.

182 **TSM-6 :** Compared to TSM-8, angle thickness of TSM-6 decreased to 6 mm. As shown in Fig.
183 10, the YL of 9.3 kN, which is about 68.9 % of that of TSM-8, is measured at a DLC of 19 mm. The
184 PL of 34.0 kN was measured at a DLC of 289 mm. At this displacement stage, the bottom angle near
185 the right side of the middle column fractured. Different to TSM-8, the load resistance of TSM-6 kept
186 decreasing after the angle fracture first occurred due to the remaining angles fractured soon. Similar to
187 TSM-8, the fracture of the angle in the second story was later than that in the ground story. Moreover,

188 the fracture of the angle near the middle column was occurred earlier than that near the side column.
189 The failure mode of TSM-6 is shown in Fig. 11.

190 **TSM-10 :** Compared to TSM-8, thicker angle of 10 mm was used in TSM-10. The YL of 21.4
191 kN, which is about 158.5 % and 230.1 % of that of TSM-8 and TSM-6, is measured at a DLC of 23
192 mm. The greater YL measured in TSM-10 is mainly because that the first yield was measured at the
193 beam flange, rather than at the angle. Different to TSM-8 and TSM-6, the load resistance kept
194 increasing until the DLC reached 425 mm due to tear failure of the beam flange near the middle column
195 in the ground story. The PL of TSM-10 is 106.2 kN, which is 239.2 % and 312.4 % of that of TSM-8
196 and TSM-6, respectively. Further increasing DLC to 483 mm, the top angle near the side column in
197 the second story fractured. After that, the fracture of angle occurred in sequence. The failure mode of
198 TSM-10 was presented in Fig. 12. Different to TSM-8 and TSM-6, tear failure of the beam flanges
199 near the middle column in the ground story was observed.

200 **Horizontal reaction force**

201 Fig. 13 shows the horizontal reaction force (negative and positive values represent compressive
202 and tensile reaction force, respectively.) From the figure, initial compressive reaction force was
203 measured in TSP and TSM specimens. Thus, compressive arch action actually was developed in the
204 beams either subjected to a penultimate column or interior column scenario. The maximum
205 compressive reaction force in TSP-8, TSM-8, TSM-6, and TSM-10 was -12.4 kN, -13.4 kN, -12.1 kN,
206 and -16.1 kN, respectively. Therefore, even without overhanging beams, TSP-8 developed similar
207 compressive arch action as that of TSM-8. Increasing the thickness of steel angle will not enhance
208 compressive arch action significantly. However, for TSM-10, as the first yield was occurred at the
209 beam flange rather than the steel angle, larger yield load and compressive arch action developed. As
210 the compressive reaction force is relatively low, the compressive arch action is insignificant, which
211 agrees with the findings from previous studies (Yang and Tan 2013a, b). As the span/depth ratio in
212 steel beams are much larger than that of reinforced concrete beams, compressive arch action for tested
213 specimens is insignificant. Therefore, in later discussion, the compressive arch action was included in

flexural action. Moreover, for all specimens, majority of compressive reaction force was attributed to the bottom pin support except for TSM-6, which was mainly attributed to the second story. In large deformation stage, tensile reaction force was measured including TSP-8. The maximum tensile reaction force of TSP-8, TSM-8, TSM-6, and TSM-10 was 27.0 kN, 82.7 kN, 57.9 kN, and 179.7 kN, respectively. Thus, contrary to compressive arch action, without overhanging beams in TSP-8 resulted in much lower tensile reaction force and catenary action. Moreover, increasing the thickness of the steel angle could increase catenary action significantly. For TSM-10, much greater catenary action was developed mainly due to the thicker angle changed the failure mode of the specimen (fracture of the beam flange, rather than fracture of the steel angle). Different to compressive reaction force, the tensile reaction force was almost provided by the bottom pin support and second story equally.

Deformation measurements

As shown in Fig. 14, outward movements were observed initially through horizontally installed LVDTs. Compared to the joints without overhanging beams, the joints with overhanging beams showed lower outward movements (refer to Fig. 14a). Moreover, the joint in the second story achieved greater outward movements than that in the first story. Similarly, greater inward movements were measured in the joints without overhanging beams. Compared to TSP-8, TSM-8 measured much lower outward movements, as shown in Fig. 14b. However, the inward movements of TSM-8 actually were greater than that of the joints with overhanging beams in TSP-8. This is mainly due to greater tensile force developed in TSM-8, which pulled the steel angle to achieve greater horizontal deformation. As shown in Figs. 14b-d, TSM-8, TSM-6, and TSM-10 achieved similar inward movements in the joints. This could be explained that although TSM-10 developed the largest tensile force, the steel angle in TSM-10 has largest horizontal stiffness. Similarly, the tensile force in TSM-6 is least. However, 6 mm thickness angle in TSM-6 resulted in the lowest horizontal stiffness. Therefore, the maximum inward movement of TSM-6, TSM-8, and TSM-10 is similar.

Fig. 15 shows the deflection shape of the beams with various stages. As shown in Fig. 15a, for TSP-8, the deformation shape of the beam in corner bay close to the deformation of a cantilever beam

240 under a concentrated load. The chord rotation, which is defined as the ratio of DLC to beam span, will
241 overestimate the rotation of the beam near the interior column but under-estimate the rotation of the
242 beam end near the lost corner column. However, different to TSC-8, as shown in Fig. 15b, double
243 curvature deformation shape was observed in TSM-8. Conversely, the chord rotation could accurately
244 estimate the rotation of the beam near the side column but over-estimate the rotation of the beam near
245 the middle column. Furthermore, the deformation was concentrated at the angles rather than the beams.
246 Similar phenomenon was found in previous studies (Hasan et al. 2017; Kong and Kim 2017). For TSP-
247 8, TSM-6, and TSM-10, similar results were observed.

248 **Internal force measurements**

249 To further understand the load resisting mechanism, the internal forces, such as axial force and
250 bending moment in beams, should be quantified from the test results. The reliability of strain gauge
251 results to determine the load resistance of tested specimens was first evaluated. The calculation method
252 has been described in detail in authors' previous work (Qian et al. 2020a). As shown in Fig. 2b, strain
253 gauges installed in Sections A1-4 or A1-8 were utilized for bending moment calculation while strain
254 gauges installed in Sections B1-4 or B1-8 were utilized for determination of the axial force. Figs. 16
255 and 17 compare the vertical load-displacement curves and horizontal reaction force-displacement
256 curves based on the results of load cell and strain gauges, respectively. From the figures, it was found
257 that, generally, the analytical results from strain gauge readings agree with the measured value from
258 load cells well, except at the location of fracture in either steel angle or beam flanges. Therefore, the
259 strain gauge results are reliable to be used in further discussion.

260 Based on strain gauge results, Fig. 18 illustrates the de-composition of load resistance from
261 different load resisting mechanisms. As shown in Fig. 18a, for TSC-8, the load resistance purely relied
262 on flexural action during test. For TSP-8, as shown in Fig. 18b, considerable catenary action was
263 developed even one side column did not have overhanging beams (no horizontal constraints from
264 surrounding bays). The maximum contribution of catenary action is 48.1 % for TSP-8. However, before
265 fracture of the steel angle, majority of the load resistance was also attributed into flexural action.

For TSM-series specimens, similar to TSP-8, catenary action was kicked-in in large deformation stage. Compared to TSP-8, the contribution of catenary action in large deformation stage was much greater. The maximum contribution of catenary action of TSM-8, TSM-6, and TSM-10 was 358.4 %, 95.6 %, and 124.6 %, respectively. The contribution of catenary action was even larger than the total load resistance, which could be explained by the contribution of flexural action was negative in large deformation stage, which can be explained as the compressive angle become tensile angle after the original tensile angle was fractured.

DISCUSSION OF TEST RESULTS

Load resistance capacity at different stories

Unlike previous studies (Sadek et al. 2011; Yang and Tan 2013a; Wang et al. 2016; Zhong et al. 2020), two-story sub-frames was fabricated and tested in this study to evaluate the difference of the development of load resisting mechanisms in different stories. Thus, based on the strain gauge results, the contribution of load resistance from different stories was determined and presented in Fig. 19. As shown in Figs. 19a and b, for TSC-8 and TSP-8, before failure first occurred at the connection, the load resistance from the first and second story is similar. For TSM-8, TSM-6, and TSM-10, as shown in Figs. 19c, d, and e, the load resistance from the first and second story is similar at early stage of the test. However, when the DLC reached 90 mm, 125 mm, and 150 mm, the load resistance of first story exceeded that of second story for TSM-8, TSM-6, and TSM-10, respectively. To reveal the difference further, the flexural action and catenary action of each story were calculated and shown in Fig. 20. As shown in Fig. 20, the flexural action developed in the first and second story is similar prior to first fracture of the angle or beam flange. However, the catenary action developed in the first story is always greater than that in the second story. Thus, for TSC-8 and TSP-8, the load resistance from the first and second story is similar as flexural action dominated the load resistance. However, for TSM-series specimens, catenary action dominated the load resistance in large deformation stage, resulting in greater load resistance from the first story in large deformation stage.

291 **Effects of the position of column removal**

292 Fig. 5 compares the vertical load response under various column removal scenarios. The initial
293 stiffness of TSM-8 and TSP-8 was much larger than that of TSC-8. The initial stiffness of TSC-8, TSP-
294 8, and TSM-8 was 0.13, 0.55 and 0.68 kN/mm, respectively. Moreover, the PL of TSC-8, TSP-8, and
295 TSM-8 was 16.6 kN, 39.8 kN, and 44.4 kN, respectively. Thus, the initial stiffness of TSC-8 was only
296 18.9 % of that of TSM-8. This was because the beams of TSC-8 worked as cantilever beam in flexural
297 action stage, while plastic hinge was formed in two beam ends in TSM-8. Thus, for TSC-8, the number
298 of plastic hinges was only 1/4 of that of TSM-8. However, the PL of TSC-8 was 37.4 % of that of
299 TSM-8. This indicated that partial plastic hinges were formed at the beam end near the corner
300 connection of TSC-8 due to Vierendeel action. Therefore, for a moment resisting frame, the Vierendeel
301 action should be considered to evaluate the load resisting capacity of the frames subjected to the loss
302 of a corner column scenario. However, majority of existing tests (Stylianidis et al. 2016b; Hou et al.
303 2016; Wang et al. 2017) conservatively treated the beam as a cantilever beam in corner column removal
304 scenario. This is because these tests based on single-story beam-column sub-assemblages, it is unable
305 to replicate the interaction between the structural components in different stories (merit of Vierendeel
306 action) well. The initial stiffness and PL of TSP-8 is 80.9 % and 89.6 % of that of TSM-8. It indicated
307 that the lack of horizontal constraints would slightly decrease the load resistance of the specimen. The
308 vertical displacement corresponding PL of TSC-8, TSP-8, and TSM-8 was 310 mm, 564 mm, and 394
309 mm, respectively. Thus, the vertical displacement corresponding PL of TSC-8 was only 78.7% of that
310 of TSM-8. However, the vertical displacement corresponding PL of TSP-8 was 143.1% of that of TSM-
311 8 due to the side column without horizontal constraints were able to move inwards to the middle column
312 in the large deformation stage, which would effectively delay the fracture of steel angle. Analyzing the
313 results, the loss of a corner column is the most critical scenario among all the cases. As shown in Fig.
314 18a, the absence of adequate horizontal constraints in the case of corner column removal, resulting in
315 limited catenary action developed, which is the second line of defense.

4.3. Effects of angle thickness

Fig. 10 illustrates the effects of angle thickness on the performance of steel frames. The initial stiffness of TSM-6, TSM-8, and TSM-10 was 0.49, 0.68 and 1.12 kN/mm, respectively. Compared to TSM-8, the initial stiffness of TSM-6 decreased by 27.9 % while TSM-10 increased by 64.7 %. In addition, the PL of TSM-6, TSM-8, and TSM-10 was 34.0 kN, 44.4 kN, and 106.2 kN, respectively. The increasing the angle thickness from 6 mm to 8 mm, the PL only increased by 30.6 %. However, increasing the angle thickness from 8 mm to 10 mm, the PL could increase by 139.2 %. This is because, compared to TSM-8, TSM-10 was failed at the beam flange, rather than at the steel angle. Furthermore, the DLC corresponding PL of TSM-6, TSM-8, and TSM-10 was 289 mm, 394 mm, and 425 mm, respectively. Thus, increasing the angle thickness, the deformation capacity of the steel frame was also increased. It should be emphasized that different from TSM-6 and TSM-8, which were fractured at the heel of the angle, for TSM-10, the plastic hinges were formed along the bolt center-lines, which increased the deformation capacity (Yang and Tan 2012; Pirmoz et al. 2009).

ANALYTICAL ANALYSIS

Although experimental tests were performed to investigate the influences of different column missing scenarios and angle thickness, as the number of tested specimens is relatively few, an analytical model was developed here to further understand the capacity of steel frames with top-and-seat angle connections to resist progressive collapse.

Middle column removal

Based on analysis of the test results, the load resistance of steel frames could be calculated by summation of the load resistance from flexural action and catenary action, as expressed by Eq. 1. Considering the difference between different stories, in this analytical model, it was assumed similar flexural action developed in different stories while the discrepancy on catenary action was considered.

$$P^{middle} = P_{FA} + P_{CA} \quad (1)$$

Flexural action

For flexural action resistance, a bilinear moment-rotation model was adopted by assuming force-deformation characteristics at both sides of connections was identical, as shown in Fig. 21.

343 According to (Bruneau et al. 1997), the yield moment of an angle leg section is 0.667 times its
 344 plastic moment. The connection yield moment can be expressed by Eq. 2:

$$345 \quad M_y = M_p / 1.5 \quad (2)$$

346 An equation from Pirmoz et al. (2009) is used to evaluate the plastic moment of the connection:

$$347 \quad M_p = \frac{\beta M_{p-angle}}{g} h_b \quad (3)$$

348 where β is the parameter used to accurately estimate the effect of variates that affect the pattern
 349 of mechanism which can be found in Pirmoz et al. (2009), $M_{p-angle}$ is the plastic moment capacity of
 350 the tensile angle leg which can be calculated by Eq. 4; g is the gage distance of the tensile angle as
 351 shown in Fig. 22a, h_b is the beam depth.

352 The plastic moment capacity of the tensile angle with material strength f_y , width b , and thickness
 353 t , can be determined as follow:

$$354 \quad M_{p-angle} = \frac{f_y b t^2}{4} \quad (4)$$

355 As suggested by Pirmoz et al. (2009), the initial stiffness K_i and the tangent stiffness of the
 356 connection K_{py} can be calculated by Eqs. 5-7.

$$357 \quad K_i = h_b^2 K_{ta} \quad (5)$$

$$358 \quad K_{ta} = \frac{1}{\frac{1}{\alpha K_1} + \frac{1}{K_3}} \quad (6)$$

$$359 \quad K_{py} = (c\alpha - d) K_i \quad (7)$$

360 In above equations, K_{ta} is the equivalent stiffness of the springs of the tensile angle vertical leg
 361 (K_1), the bolt axial stiffness (K_2), and the bolt flexural stiffness (K_3) in series, as shown in Fig. 22b.
 362 Ignoring axial deformation of the column bolts, K_{top} can be calculated by Eq. 6. α is a modification
 363 factor for the flexural stiffness; c and d are the parameters to consider the effects of different material
 364 properties. The equations for determination of K_1 , K_3 , α , c , and d can be found from Pirmoz et al.
 365 (2009) in detail.

366 Before the connection yielding, the load resistance of the frame was only provided by flexural
 367 action. For the specimens under middle column removal scenario, the yield displacement u_y^{middle} and
 368 yield load P_y^{middle} were determined by Eqs. 8 and 9, respectively.

$$369 \quad u_y^{middle} = M_y L / K_i \quad (8)$$

$$370 \quad P_y^{middle} = 2 \times 2 \times \frac{2M_y}{L} \quad (9)$$

371 where L is the span length.

372 In post yield stage, the relationship between vertical displacement u and flexural action as shown
 373 in below:

$$374 \quad M_{py} = M_y + \frac{K_{py} (u - u_y^{middle})}{L} \quad (10)$$

$$375 \quad P_{FA}^{middle} = 2 \times 2 \times \frac{2M_{py}}{L} \quad (11)$$

376 **Catenary action**

377 Assuming the column with sufficient horizontal constraints have full connectivity with the angle,
 378 the axial deformation of the beams can be determined based on the second-order approximation and
 379 expressed as Eq. 12 (Stylianidis et al. 2016a), as shown in Fig. 23a. It should be noted that the axial

380 deformation of the beam is twice the deformation of a single angle connection as a beam has two angle
 381 connection.

$$382 \quad \Delta = \Delta^b / 2 = L(1 - \cos \theta) / 2 = u^2 / (4L) \quad (12)$$

383 It should be noted that catenary action began to develop once the axial deformation exceeded the
 384 gap in the angle connection. As the designed allowance of bolts was 1 mm, the gap related to axial
 385 deformation (Δ_{gap}^{1st}) is 2 mm for the beams in the first story. As the gaps in the first story will affect the
 386 formation of catenary action in the second story, the gap (Δ_{gap}^{2nd}) is 4 mm for the beams in the second
 387 story. The behavior of spring load-deformation relationship is shown in Fig. 23b. Based on the force
 388 equilibrium, the catenary action of each story can be calculated according to Eq. 13.

$$389 \quad P_{CA} = \frac{K_s (u - u_{\Delta gap})^3}{L^2} \quad (13)$$

390 where K_s is the spring stiffness, which will be introduced in detail as following; $u_{\Delta gap}$ is the
 391 vertical displacement in accordance with Δ_{gap} ($u_{\Delta gap} = \sqrt{4L\Delta_{gap}}$ based on Eq. 12).

392 For TSM-6 and TSM-8, the failure mode was controlled by angle fracture. The elastic stiffness of
 393 the spring in the ground story K_s^{1st} , as proposed by Faella et al. (2000), can be determined as Eq. 14.

$$394 \quad K_s^{1st} = K_{at} = \frac{0.5b_{eff}t^3E}{m^3} \left(\frac{4\gamma}{4\gamma + 3} \right) \quad (14)$$

395 where b_{eff} is the effective width of the angle which can be obtained in Faella et al. (2000), E is
 396 the Young's modulus, the geometric parameter m and the coefficient $\gamma = \frac{I_2/L_2}{I_1/L_1}$ are shown in Fig. 24.

397 Based on experimental results, the elastic stiffness of the spring in the second story (K_s^{2nd}) is
 398 about 0.4 of that of K_s^{1st} . It was assumed that the specimen reached its ultimate capacity when the axial

399 force of ground story $N^{1st} = P_{CA}^{1st} / \sin \theta$ exceeds the bending resistance of the tensile angle ($F_{T,Rd}$), as
 400 shown in Eq. 15.

$$401 \quad F_{T,Rd} = \frac{4M_{y,Rd}}{m} = \frac{b_{eff} t^2 f_y}{m} \quad (15)$$

402 For TSM-10, as fracture occurred at the beam flange, rather than at a steel angle. The spring
 403 stiffness K_s' (to distinguish K_s is Eq. 13) should be determined as Eq. 16, where the stiffness of angle
 404 in tension (K_{at}), the stiffness of beam flange in bearing (K_{fb}), and the stiffness of angle in bearing
 405 (K_{ab}) are equivalently considered.

$$406 \quad K_s' = \frac{1}{\frac{1}{K_{at}} + \frac{1}{K_{fb}} + \frac{1}{K_{ab}}} \quad (16)$$

407 where K_{at} could be determined by Eq. 14, K_{fb} and K_{ab} could be determined by Eq. 17, as
 408 suggested by Rex et al. (2003). It should be noted that Eq. 17 is proposed for bearing stiffness of a
 409 single plate with a single bolt. For tested angle, two bolts were utilized. Thus, K_b should be $2K_b'$ herein.
 410 Moreover, for K_{fb} and K_{ab} , the geometric and material properties of beam flange and angle were
 411 utilized, respectively.

$$412 \quad 2K_b' = 2 \left(\frac{1}{\frac{1}{K_{br}} + \frac{1}{K_b} + \frac{1}{K_v}} \right) \quad (17)$$

413 The bearing stiffness $K_{br} = 120 t_p f_{yp} (d_b / 25.4)^{0.8}$, bending stiffness $K_b = 32 E_p t_p (L_e / d_b - 0.5)^3$ and
 414 shear stiffness $K_v = 6.67 G_p t_p (L_e / d_b - 0.5)$; in which G_p is the shear modulus of the steel plate, L_e is
 415 the distance from bolt center to plate edge.

416 For TSM-10, it was assumed that failure occurred when the beam axial force exceeded the bearing
 417 capacity of the beam flange, as shown in Eq. 18 (Liu et al. 2015).

$$418 \quad F_{fb,Rd} = \min(L_e, 2.76d_b) \times f_{yf} t_f \quad (18)$$

419 **Penultimate column removal**

420 The stiffness of horizontal constraints of the steel frame subjected to the loss of a penultimate
 421 column scenario was determined by the side column without overhanging beams. Thus, it was not
 422 accurate to assume similar horizontal constraints to that from the side column with overhanging beams.
 423 For simplicity, a reduction coefficient of $\lambda=0.75$ is assumed to related to the case of loss middle
 424 column scenario. Similar to the case of loss of a middle column, it was assumed that the specimen
 425 failure when the axial force of ground story $N^{1st} = P_{CA}^{1st} / \sin \theta$ exceeds the bending resistance of tensile
 426 angle ($F_{T,Rd}$), as shown in Eq. 15. Thus, the load resistance of the frame subject to the loss of a
 427 penultimate column was determined by Eq. 19.

$$428 \quad P^{penultimate} = \lambda P^{middle} \quad (19)$$

429 **Corner column removal**

430 Vierendeel action was found to resist progressive collapse in TSC-8. Thus, the corner column in
 431 the second story has partial rotational constraints to the beam end. As suggested by Qian and Li (2015),
 432 a rotational constraint effectiveness factor $\xi=0.7$ was utilized to evaluate the extent of the rotational
 433 constraints in the corner joint. The yield load of TSC-8 is determined in Eq. 20.

$$434 \quad P_y^{corner} = 2 \times \frac{(1 + \xi) M_y}{L} \quad (20)$$

435 Qian and Li (2015) indicated that the real boundary condition of the corner column removal
 436 scenario (Fig. 25c) lay between the full (Fig. 25a) and free constraints (Fig. 25b). For full rotational
 437 constraint mode I ($\xi=1$), the yield displacement is expressed as below:

$$u_y^{full} = \frac{\phi_y}{6} L^2 \quad (21)$$

where ϕ_y is the yield curvature at fixed support in Fig. 25a.

For partial rotational constraint model ($\xi=0.7$), the yield displacement is expressed as below:

$$u_y^{partial} = \frac{\phi_y L^2}{6} (2 - \xi) \quad (22)$$

Thus, yield displacement under corner column removal scenario can be expressed as in Eq. 23.

$$u_y^{corner} = \frac{u_y^{partial}}{u_y^{full}} u_y^{middle} = (2 - \xi) u_y^{middle} \quad (23)$$

As flexural action is considered in the prediction of TSC-8 and the progressive collapse resistance in post yield stage can be expressed as in Eq. 24.

$$P_{py}^{corner} = 2 \times \frac{(1 + \xi) M_{py}}{L} \quad (24)$$

Similarly, for TSC-8, the vertical displacement corresponding the first fracture can be expressed as in Eq. 25.

$$u_{FF}^{corner} = (2 - \xi) u_{FF}^{middle} \quad (25)$$

where $u_{FF}^{middle} = \sqrt[3]{\frac{F_{t,Rd} L^2 \sin \theta}{K_s}} + u_{\Delta gap}^{1st}$ is the vertical displacement corresponding the first fracture

of TSM-8.

Verification of analytical model

Fig. 26 compares the analytical load-displacement curve of tested specimens with those from tests. The key results of these curves are tabulated in Table 4. In general, the analytical models predict

455 the initial stiffness, yield load, and first fracture of the steel angle or beam flange well. However, the
456 analytical models could not predict the decreasing of the load resistance after first fracture.

457 **CONCLUSIONS**

458 In this paper, five two-story steel sub-frames with top-and-seat connections were tested under
459 different column missing scenarios. A series of analytical models were adopted and further developed
460 to predict the load resisting capacity of tested specimens. Based on experimental and analytical results,
461 conclusions are drawn:

- 462 1. It was found that the load resisting capacity and deformation capacity of TSC-8 are only 37.4 %
463 and 78.7 % of that of TSM-8. TSP-8 achieved 89.6 % of the load resisting capacity of TSM-8.
464 However, Compared to TSM-8, the deformation capacity of TSP-8 increased by 43.1 %.
- 465 2. The load resisting mechanisms of TSP-8 are similar to that of TSM-8, flexural action and
466 catenary action were able to develop to resist progressive collapse. However, catenary action
467 of TSP-8 was commenced much later than TSM-8. For TSC-8, only flexural action is developed
468 during test. Moreover, the partial rotational constraints from the corner column in the second
469 story due to Vierendeel action should be considered for determination of flexural action of the
470 frame under the loss of a corner column scenario.
- 471 3. When the angle thickness increased from 6 mm to 8 mm, the load resisting capacity increased
472 by 30.6 %. However, when the angle thickness increased from 8 mm to 10 mm, the load
473 resisting capacity increased by 139.2 %, which is mainly due to the thicker angle changed the
474 failure mode of the frame from angle fracture to the fracture of the beam flange.
- 475 4. Test results indicated that, an effective way to improve the performance of steel moment frames
476 against progressive collapse by increasing the angle thickness. Moreover, considering the
477 beneficial of large deformation capacity, which is important for development of catenary action,
478 of the frame with top-and-seat angle connection, the performance of the frames with top-and-
479 seat angle connection against progressive collapse was reliable and should be recommended.
- 480 5. The rotational constraint difference between the first and second story has little influence on

the flexural action. Thus, similar load resistance developed in the first and second story before first fracture occurred. However, compared with second story, the larger horizontal constraints for the beams in the ground story resulted in greater catenary action developed in the first story. Multi-story sub-frames were recommended for investigation on behavior of moment frames to resist progressive collapse, especially for the scenario of loss of a corner column.

6. Proposed analytical analysis could reasonably predict the load-displacement curve before the first fracture occurred in the angle or beam flange. However, the models are unable to predict the softening part of the load-displacement curve.

ACKNOWLEDGEMENTS

This research was supported by a research grant provided by the Natural Science Foundation of China (Nos.52022024, 51778153). Any opinions, findings and conclusions expressed in this paper are those of the writers and do not necessarily reflect the view of Natural Science Foundation of China.

DATA AVAILABILITY

Some or all data, models, or code that support the findings of this study are available from the corresponding author upon reasonable request.

FUTURE WORK

As the slab may affect the load redistribution capacity of steel frames with different connections significantly, it was necessary to carry out more tests on three-dimensional multi-story and multi-bay steel substructures including slabs subjected to different column missing scenarios in the future. Additionally, as mentioned in the section of “Test setup”, the commonly used push-down loading method, which is ignored the uniformly distributed dead load and live load, is adopted in this study. This may affect the failure mode and deformation capacity as well as catenary action capacity of the specimens. As no studies had been carried out on steel frames for progressive collapse included or excluded the effects of uniformly distributed loads, it is necessary to do relevant studies in the future.

REFERENCES

506 Abdalla, K. M., G. A. Drosopoulos, and G. E. Stavroulakis. (2015). "Failure behavior of a top and seat
 507 angle bolted steel connection with double web angles." J. Struct. Eng. 141 (7): 04014172.
 508 Alashker, Y., and Li, H. H., Ei-Tawil, S. (2011). "Approximations in Progressive Collapse Modeling."
 509 J. Struct. Eng, 137 (9): 914-924.
 510 ANSI (2005). "Specification for Structural Steel Buildings." ANSI/AISC 360-16. Chicago, Illinois,
 511 USA.
 512 Azizinamini, A. (1982). "Monotonic Response of Semi-Rigid Steel Beam to Column Connections."
 513 M.Sc. thesis, College of Engineering, Univ. of South Carolina.
 514 Beland, T., Tremblay, R., Hines, E. M., and Fahnestock L. A. (2020a). "Rotational Capacity of Bolted
 515 Double-Web-Angle Beam-Column Gravity Connections through Full-Scale Experimental Testing."
 516 J. Struct. Eng. 146(7): 04020111.
 517 Beland, T., Tremblay, R., Hines, E. M., and Fahnestock L. A. (2020b). "Full-Scale Cyclic Rotation
 518 and Shear-Load Testing of Double Web with Top and Seat Angle Beam-Column Connections." J.
 519 Struct. Eng. 146(8): 04020164.
 520 Beland, T., Bradley, C. R., Nelson J., Sizemore J. G., Davaran, A., Tremblay, R., Hines, E. M., and
 521 Fahnestock L. A. (2020c). "Experimental Parametric Characterization of Bolted Angle Connection
 522 Behavior." J. Struct. Eng. 146(8): 04020160.
 523 Bruneau, M., Uang, C. M., and Whittaker, A. (1997). "Ductile Design of Steel Structures." New York
 524 (NY): McGraw-Hill: 480.
 525 Davaran, A., Beland, T., and Tremblay, R. (2019). "Elastic-Plastic Analysis of Bolted Angles Usable
 526 in Steel Frame Connections." J. Struct. Eng. 145(7): 04019048.
 527 Danesh, F., A. Pirmoz, and A. S. Daryan. (2007). "Effect of Shear Force on the Initial Stiffness of Top
 528 and Seat Angle Connections with Double Web Angles." J. Constr. Steel Res. 63 (9): 1208–1218.
 529 Dimopoulos, C. A., Freddi, F., Karavasilis, T. L., and Vasdravellis, G., (2020). "Progressive Collapse
 530 Resistance of Steel Self-Centering MRFs Including the Effects of the Composite Floor." Eng.
 531 Struct. 206: 110143.

532 Dinu, F., Marginean, I., and Dubina, D. (2017). "Experimental Testing and Numerical Modelling of
533 Steel Moment-Frame Connections under Column Loss." Eng. Struct. 150: pp. 861-878.

534 Dinu, F., Marginean, I., Dubina, D., and Petran, I. (2016). "Experimental Testing and Numerical
535 Analysis of 3D Steel Frame System under Column Loss." Eng. Struct. 113: 59-70.

536 DoD (2010). "Design of Building to Resist Progressive Collapse." UFC 4-023-03. Washington, DC,
537 USA.

538 Faella, C., Piluso, V., and Rizzano, G. (2000). "Structural Steel Semirigid Connections: Theory, Design
539 and Software." New directions in civil engineering. Boca Raton (FL (EEUU)). CRC Publishers.

540 Fu, F. (2009). Progressive collapse analysis of high-rise building with 3-D finite element modeling
541 method. Journal of Constructional Steel Research, 65(6), pp. 1269–1278

542 Fu, F. (2010). 3-D nonlinear dynamic progressive collapse analysis of multi-storey steel composite
543 frame buildings — Parametric study. Engineering Structures, 32(12), pp. 3974–3980

544 Fu, F. (2012). "Response of a Multi-Storey Steel Composite Building with Concentric Bracing under
545 Consecutive Column Removal Scenarios." J. Constr. Steel Res. 70: 115–126.

546 Gao, S., Guo, L. H., Fu F, and Zhang, S. (2017). "Capacity of Semi-Rigid Composite Joints in
547 Accommodating Column Loss." J. Constr. Steel Res. 139: 288-301.

548 Gong, Y. (2014). "Ultimate Tensile Deformation and Strength Capacities of Bolted-Angle
549 Connections." J. Constr. Steel Res. 100 (6): 50–59.

550 Gong, Y. (2017). "Test, Modeling and Design of Bolted-Angle Connections subjected to Column
551 Removal." J. Constr. Steel Res. 139: 315–326.

552 Garlock, M., J. M. Ricles, and R. Sause. (2003). "Cyclic Load Tests and Analysis of Bolted Top-and-
553 Seat Angle Aonnections." J. Struct. Eng. 129 (12): 1615–1625.

554 GSA (2013). "Progressive Collapse Analysis and Design Guidelines for New Federal Office Buildings
555 and Major Modernization Projects." Washington, DC, USA.

556 Hasan, M. J., Ashraf, M., and Uy, B. (2017). "Moment-Rotation Behaviour of Top-Seat Angle Bolted
557 Connections Produced from Austenitic Stainless Steel." J. Constr. Steel Res. 136 (2): 149-161.

558 Hou, J., Song, L., and Liu, H. H. (2016). "Testing and Analysis on Progressive Collapse-Resistance
559 Behavior of RC Frame Substructures under a Side Column Removal Scenario." *J. Perform. Constr.*
560 *Facil.* 30 (5): 04016022.

561 Khandelwal, K., and Ei-Tawil, S. (2007). "Collapse Behavior of Steel Special Moment Resisting
562 Frame Connections." *J. Struct. Eng.* 133 (5): 646-655.

563 Kong, Z. Y., and Kim, S. E. (2017). "Numerical Estimation for Initial Stiffness and Ultimate Moment
564 of Top-Seat Angle Connections without Web Angle." *J. Struct. Eng.* 143 (10): 04017138.1-
565 04017138.15.

566 Lee, C. H., Kim, S., and Lee, K. (2010). "Parallel Axial-Flexural Hinge Model for Nonlinear Dynamic
567 Progressive Collapse Analysis of Welded Steel Moment Frames." *J. Struct. Eng.* 136 (2): 165-173.

568 Lew, H. S., Main, J. A., Robert, S. D., Sadek, F., and Chiarito, V. P. (2013). "Performance of Steel
569 Moment Connections under a Column Removal Scenario. I: Experiments." *J. Struct. Eng.* 139 (1):
570 98-107.

571 Li, H. H., Cai, X. H., Zhang, L., Zhang, B. Y., and Wang, W. (2017). "Progressive Collapse of Steel
572 Moment-Resisting Frame Subjected to Loss of Interior Column: Experimental Tests." *Eng. Struct.*
573 150: 203-220.

574 Li, L., Wang, W., Chen, Y. Y., and Teh, L. H. (2007). "Column-Wall Failure Mode of Steel Moment
575 Connection with Inner Diaphragm and Catenary Mechanism." *Eng. Struct.* 131: 553-563.

576 Li, L. L., Li, G. Q., Jiang, B. H., and Lu, Y. (2018). "Analysis of Robustness of Steel Frames against
577 Progressive Collapse." *J. Constr. Steel Res.* 143: 264-278.

578 Liu, C., Tan, K. H., and Fung, T. C. (2015). "Component-Based Steel Beam-Column Connections
579 Modelling for Dynamic Progressive Collapse Analysis." *J. Constr. Steel Res.* 107: 24-36.

580 Liu, C., Tan, K. H., and Fung, T. C. (2015). "Investigations of Nonlinear Dynamic Performance of
581 Top-And-Seat with Web Angle Connections Subjected to Sudden Column Removal." *Eng. Struct.*
582 99: 449-461.

583 Lu, X. Z., Zhang, L., Lin, K. Q., and Li, Y. (2019). "Improvement to Composite Frame Systems for
584 Seismic and Progressive Collapse Resistance." *Eng. Struct.* 186: 227-242.

585 Meng. B., Zhong, W. H., Hao, J. P., Song, X. Y., and Tan, Z. (2019). "Calculation of the Resistance
 586 of an Unequal Span Steel Substructure Against Progressive Collapse Based on the Component
 587 Method." *Eng. Struct.* 182: 13-28.

588 Oosterhof, S. A. and Driver, R. D. (2015). "Behavior of Steel Shear Connections under Column
 589 Removal Demands." *J. Struct. Eng.* 141(4): 04014126.

590 Weigand, J. M. and Berman, J. W. (2016). "Integrity of Bolted Connections Subjected to Simulated
 591 Column Removal." *J. Struct. Eng.* 142(3): 04015165.

592 Pirmoz, A., Khoei, A. S., Mohammadrezapour, E., and Daryan, A. S. (2009). "Moment-Rotation
 593 Behavior of Bolted Top-Seat Angle Connections." *J. Constr. Steel Res.* 65 (4): 973-984.

594 Qian, K., and Li, B. (2015). "Analytical Evaluation of the Vulnerability of RC Frames for Progressive
 595 Collapse Caused by the Loss of a Corner Column." *J. Perform. Constr. Fac.* 29 (1): 04014025.

596 Qian, K., Lan, X., Li, Z., Li, Y., and Fu, F. (2020a). "Progressive Collapse Resistance of Two-Storey
 597 Seismic Configured Steel Sub-Frames Using Welded Connections." *J. Constr. Steel Res.* 170:
 598 106117.

599 Qian, K., Liang, S. L., Xiong, X. Y., Fu, F., and Fang, Q. (2020b). "Quasi-Static and Dynamic Behavior
 600 of Precast Concrete Frames with High Performance Dry Connections Subjected to Loss of a
 601 Penultimate Column Scenario." *Eng. Struct.* 205: 110115.

602 Qian, K., Liang, S. L., Feng, D. C., Fu, F., and Wu, G. (2020c). "Experimental and Numerical
 603 Investigation on Progressive Collapse Resistance of Post-Tensioned Precast Concrete Beam-
 604 Column Subassemblages." *J. Struct. Eng.*, 146(9): 04020170.

605 Qin, X., Wang, W., Chen, Y. Y., and Bao, Y. H. (2016). "A Special Reinforcing Technique to Improve
 606 Resistance of Beam-to-Tubular Column Connections for Progressive Collapse Prevention." *Eng.*
 607 *Struct.* 2016; 17: 26-39.

608 Rex, C., and Easterling, W. (2003). "Behaviour and Modelling of a Bolt Bearing on a Single Plate." *J.*
 609 *Struct. Eng.* 192 (6): 792–801.

610 Sadek, F., Main, J. A., Lew, H. S., and Bao, Y. H. (2011). "Testing and Analysis of Steel and Concrete
 611 Beam-Column Assemblies under a Column Removal Scenario." *J. Struct. Eng.* 137 (9): 881-892.

612 Shen, J., and A. Astaneh-Asl. (1999). "Hysteretic Behavior of Bolted-Angle Connections." *J. Constr.*
613 *Steel Res.* 51 (3): 201–218.

614 Shen, J., and A. Astaneh-Asl. (2000). "Hysteresis Model of Bolted-Angle Connections." *J. Constr.*
615 *Steel Res.* 54 (3): 317–343.

616 Stevens, D., Crowder, B., Sunshine, D., Marchand, K., Smilowitz, R., Williamson, E., and Waggoner,
617 M. (2011). "DoD Research and Criteria for the Design of Buildings to Resist Progressive Collapse." *J. Struct. Eng.* 137 (9): 870-880.

619 Stylianidis, P. M., Nethercot, D. A., Izzuddin, B. A., and Elghazouli, A. Y. (2016a). "Robustness
620 Assessment of Frame Structures Using Simplified Beam and Grillage Models." *Eng. Struct.* 115:
621 78–95.

622 Stylianidis, P. M., Nethercot, D. A., Izzuddin, B.A., and Elghazouli, A.Y. (2016b). "Study of the
623 Mechanics of Progressive Collapse with Simplified Beam Models." *Eng. Struct.* 117: 287-304.

624 Tang, H. Y., Deng, X. Z., Jia, Y. G., Xiong, J. G., and Peng, C. M. (2019). "Study on the Progressive
625 Collapse Behavior of Fully Bolted RCS Beam-to-Column Connections." *Eng. Struct.* 199: UNSP
626 109618.

627 Wang, H., Tan, K. H., and Yang, B. (2020). "Experimental Tests of Steel Frames with Different Beam-
628 Column Connections under Falling Debris Impact." *J. Struct. Eng.* 146 (1): 04019183.

629 Wang, J. J., Wang, W., and Qian, X. D. (2019). "Progressive Collapse Simulation of the Steel-Concrete
630 Composite Floor System Considering Ductile Fracture of Steel." *Eng. Struct.* 200: 109701.

631 Wang, W., Fang, C., Qin, X., Chen, Y. Y., and Li, L. (2016). "Performance of Practical Beam-to-SHS
632 Column Connections against Progressive Collapse." *Eng. Struct.* 106: 332-347.

633 Wang, W., Wang, J. J., Sun, X., and Bao, Y. H. (2017). "Slab Effect of Composite Subassemblies
634 under a Column Removal Scenario." *J. Constr. Steel Res.* 129: 141-155.

635 Yang, B., and Tan, K. H. (2012). "Component-Based Model of Bolted-Angle Connections Subjected
636 to Catenary Action." *Proc. of the 10th Intl. Conf. on Advances in Steel Concrete Composite and*
637 *Hybrid Structures.* 654–61.

638 Yang, B., and Tan, K. H. (2013a). “Experimental Tests of Different Types of Bolted Steel Beam-
639 Column Joints under a Central-Column-Removal Scenario.” Eng. Struct. 54: 112-130.

640 Yang, B., and Tan, K. H. (2013b). “Robustness of Bolted-Angle Connections against Progressive
641 Collapse: Experimental Tests of Beam-Column Joints and Development of Component-Based
642 Models.” J. Struct. Eng. 139 (9): 1498-1514.

643 Zhong, W. H., Tan, Z., Tian, L. M., Meng, B., Song, X. Y., and Zheng, Y. H. (2020). “Collapse
644 Resistance of Composite Beam-Column Assemblies with Unequal Spans under an Internal
645 Column-Removal Scenario.” Eng. Struct. 206: 110143.

646
647 **FIGURE CAPTIONS**

648
649 **Fig. 1.** Location of the extracted frame in the prototype building (unit in mm): (a) plan view; (b)
650 elevation view

651 **Fig. 2.** Dimensions of the specimen and locations of strain gauge and displacement transducers (unit
652 in mm): (a) arrangements of strain gauges/rosettes and displacement transducers; (b) strain gauges
653 positions on sections

654 **Fig. 3.** Geometric details of top-and-seat angle connection (unit in mm): (a) elevation view; (b) lateral
655 view

656 **Fig. 4.** Test setups: (a) Schematic view of TSM-8; (b) Schematic view of TSP-8; (c) Schematic view
657 of TSC-8; (d) Photograph of TSC-8

658 **Fig. 5.** Comparison of the load-displacement curves of specimens: TSC-8, TSP-8 and TSM-8

659 **Fig. 6.** Failure mode of TSC-8

660 **Fig. 7.** Failure mode of TSP-8

661 **Fig. 8.** Comparison of bending moment diagrams of the specimen: (a) excluding uniform load, (b)
662 including uniform load

663 **Fig. 9.** Failure mode of TSM-8

664 **Fig. 10.** Comparison of the load-displacement curves of specimens: TSM-6, TSM-8 and TSM-10

665 **Fig. 11.** Failure mode of TSM-6

666 **Fig. 12.** Failure mode of TSM-10

667 **Fig. 13.** Horizontal reaction force-middle column displacement curves: (a) TSP-8; (b) TSM-8; (c)

668 TSM-6; (d) TSM-10

669 **Fig. 14.** Horizontal movement of exterior joints: (a) TSP-8; (b) TSM-8; (c) TSM-6; (d) TSM-10

670 **Fig. 15.** Overall deflection profile of the beams in the first story: (a) TSC-8; (b) TSM-8

671 **Fig. 16.** Comparisons of the vertical load-displacement response from strain gauge and load cell: (a)

672 TSC-8, TSM-8, TSP-8, TSM-6; (b) TSM-10

673 **Fig. 17.** Comparisons of horizontal reaction force-displacement response from strain gauge and load

674 cell: (a) TSM-8, TSP-8, TSM-6; (b) TSM-10

675 **Fig. 18.** De-composition of the load resistance from different actions: (a) TSC-8; (b) TSP-8; (c) TSM-

676 8; (d) TSM-6; (e) TSM-10 (Note: FA and CA represent flexural action and catenary action,

677 respectively)

678 **Fig. 19.** De-composition of load resistance from 1st story and 2nd story: (a) TSC-8; (b) TSP-8; (c)

679 TSM-8; (d) TSM-6; (e) TSM-10.

680 **Fig. 20.** Comparisons of the bending moment and axial force variation in 1st story and 2nd stories: (a)

681 TSC-8; (b) TSP-8; (c) TSM-8; (d) TSM-6; (e) TSM-10.

682 **Fig. 21.** Moment-rotation behavior of connection.

683 **Fig. 22.** Simplification of the connection behavior: (a) idealized deformation pattern of connection; (b)

684 equivalent springs of connection components

685 **Fig. 23.** Modelling of catenary action: (a) approximation of axial deformation; (b) structural

686 representation.

687 **Fig. 24.** Tensile angle model

688 **Fig. 25.** Sketch of boundary condition assumption for analytical analysis

689 **Fig. 26.** Comparisons of test result and prediction model: (a) TSC-8; (b) TSP-8; (c) TSM-8; (d)

690 TSM-6; (e) TSM-10

691
692
693

Table 1-Specimen properties

Test ID	Column removal position	Angle section (mm)
TSC-8	Corner	L70×8
TSP -8	Penultimate	L70×8
TSM-8	Middle	L70×8
TSM-6	Middle	L70×6
TSM-10	Middle	L70×10

Table 2-Material properties

Items	Plate thickness (mm)	Yield strength (MPa)	Yield strain	Ultimate strength (MPa)	Ultimate strain	Elongation (%)
Beam flange	8.0	310	0.0019	420	0.0240	12.0
Beam web	5.5	320	0.0021	430	0.0249	13.5
Column flange	10.0	300	0.0019	410	0.0267	14.0
Column web	7.0	295	0.0023	375	0.0242	13.0
Angle 1	6.0	300	0.0018	425	0.0243	14.0
Angle 2	8.0	310	0.0019	420	0.0276	12.0
Angle 3	10.0	290	0.0018	430	0.0264	14.1

Table 3-Test results

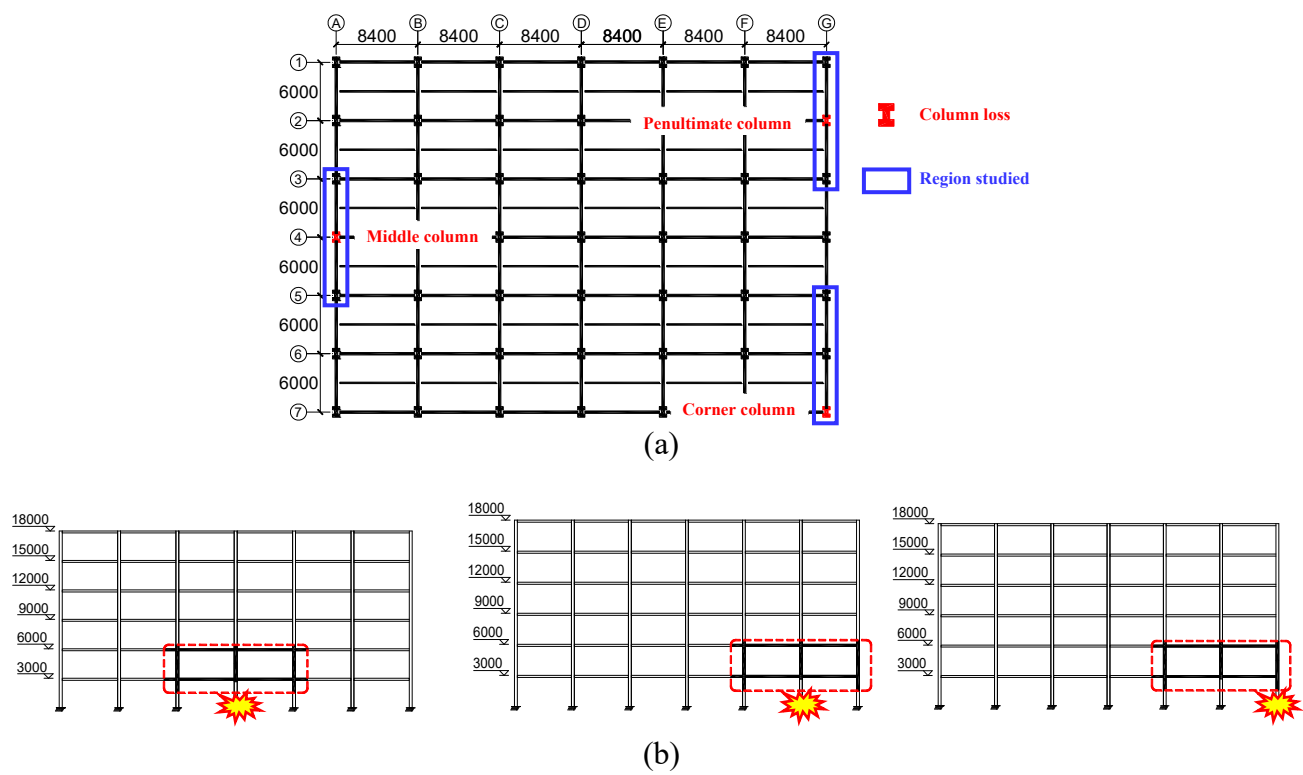
Test ID	U _{YL} (mm)	F _{YL} (kN)	K _{YL} (kN/mm)	U _{PL} (mm)	F _{PL} (kN)
TSC-8	40	5.1	0.13	310	16.6
TSP -8	20	11.0	0.55	564	39.8
TSM-8	20	13.5	0.68	394	44.4
TSM-6	19	9.3	0.49	289	34.0
TSM-10	23	21.4	1.12	425	106.2

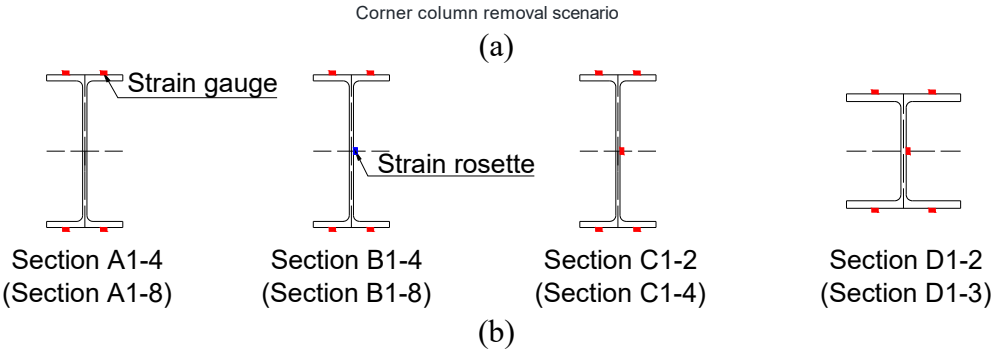
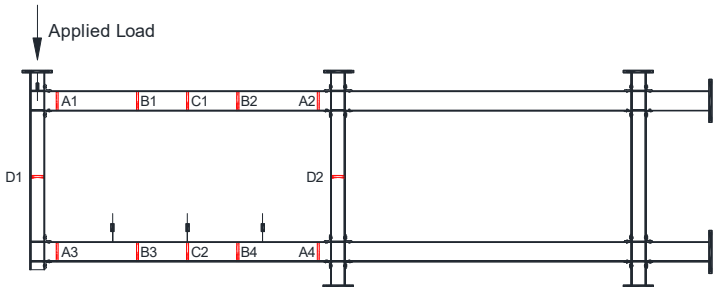
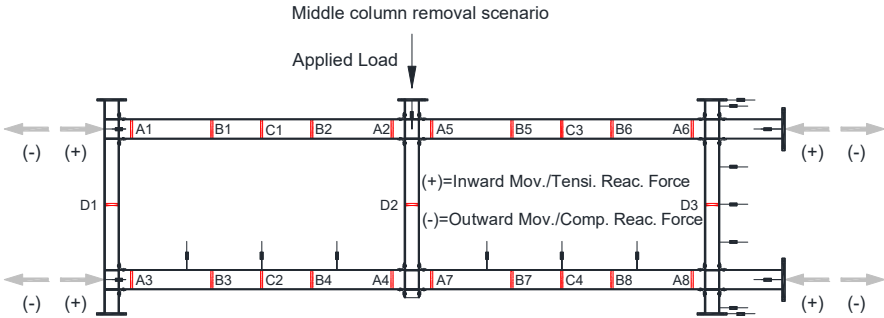
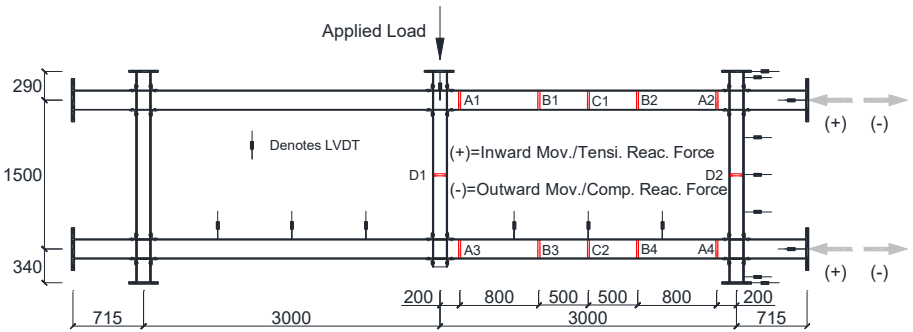
Note: F_{YL} and F_{PL} represent yield load and peak load, respectively; U_{YL} and U_{PL} represent displacements corresponding the yield load and peak load, respectively; K_{YL} represents initial stiffness corresponding the yield load

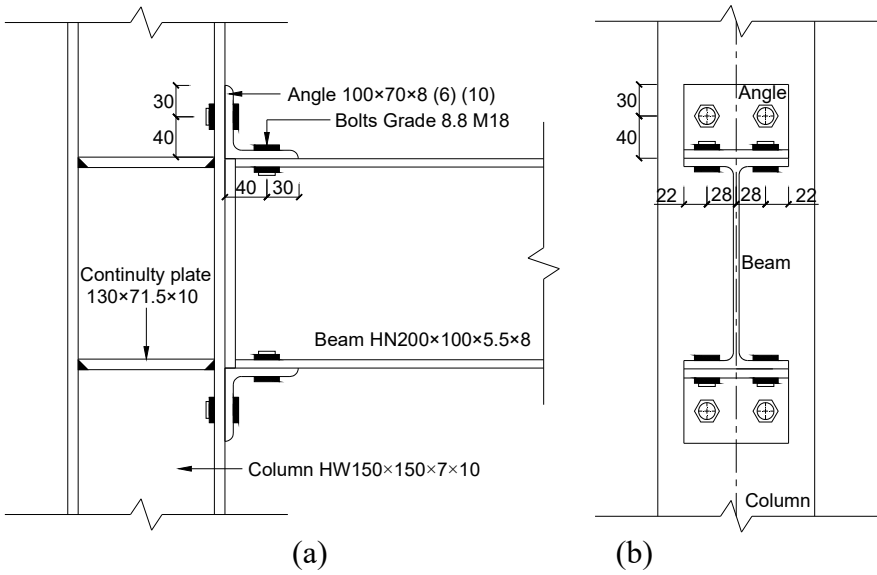
Table 4-Comparisons between test results and analytical results

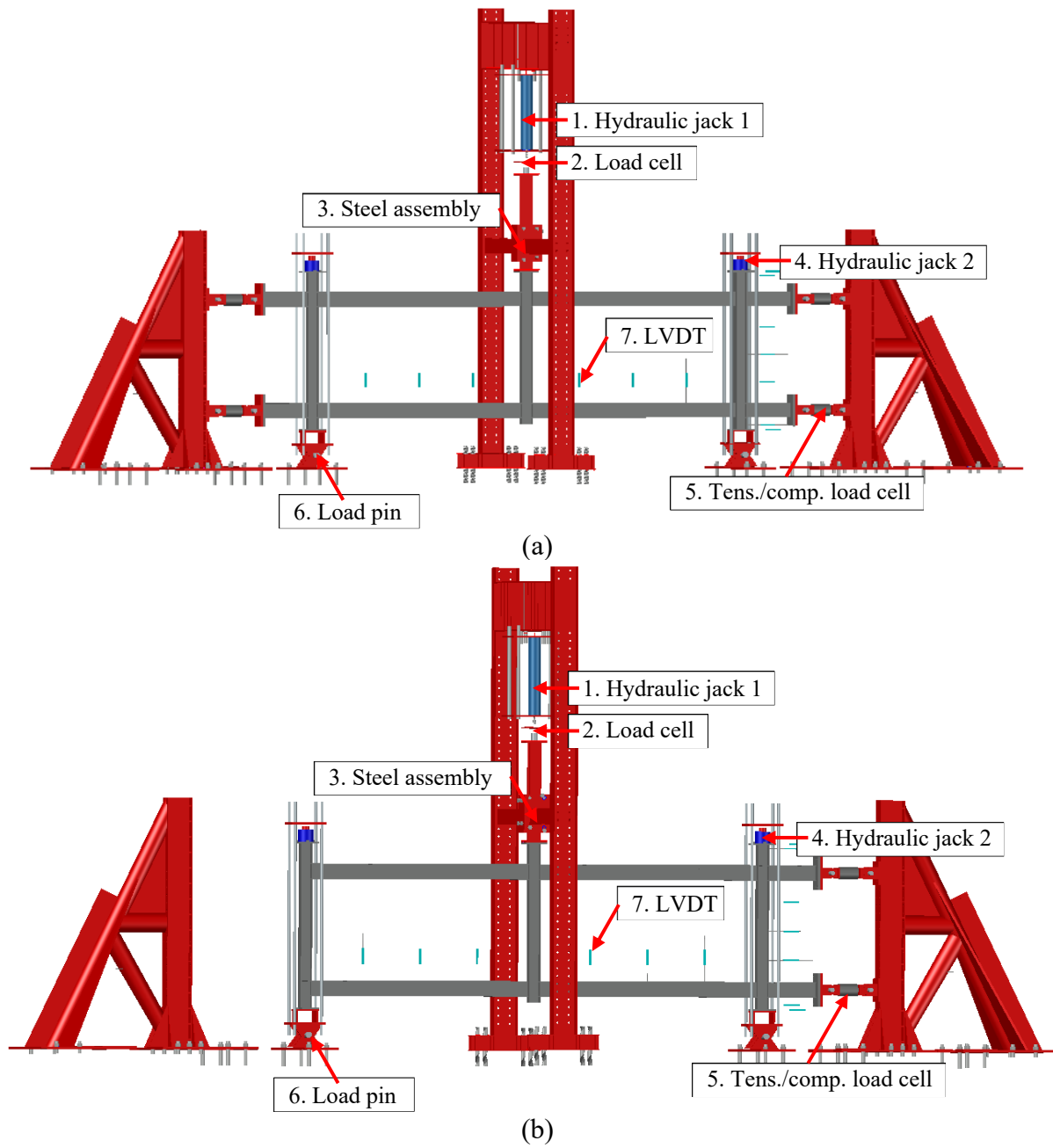
Test ID		K _{YL} (kN/mm)	Discrepancy	F _{YL} (kN)	Discrepancy	U _{FF} (mm)	Discrepancy	F _{FF} (kN)	Discrepancy
TSC-8	Test data	0.13		5.1		310		16.6	
	Analytical results	0.13	1.5%	5.2	2.1%	356	14.9%	17.6	5.8%
TSP-8	Test data	0.55		11.0		295		36.7	
	Analytical results	0.67	22.3%	14.6	32.1%	356	20.5%	36.7	0.2%
TSM-8	Test data	0.68		13.5		289		41.3	
	Analytical results	0.87	29.2%	13.0	-3.7%	274	-5.1%	40.2	-2.6%
TSM-6	Test data	0.49		9.3		289		34.0	
	Analytical results	0.75	52.9%	8.6	-7.4%	293	1.5%	35.9	5.6%
TSM-10	Test data	1.12		21.4		425		106.2	
	Analytical results	1.14	2.0%	32.0	49.5%	388	-8.8%	104.4	-1.7%

Note: U_{FF} and F_{FF} represent the vertical displacement and vertical load corresponding the first fracture









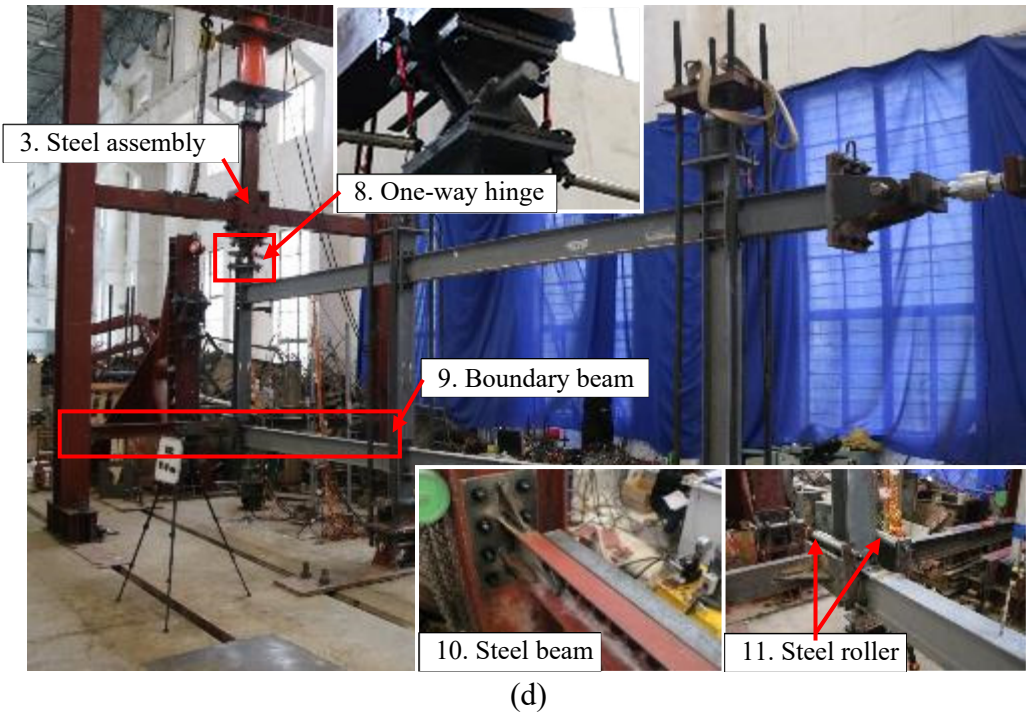
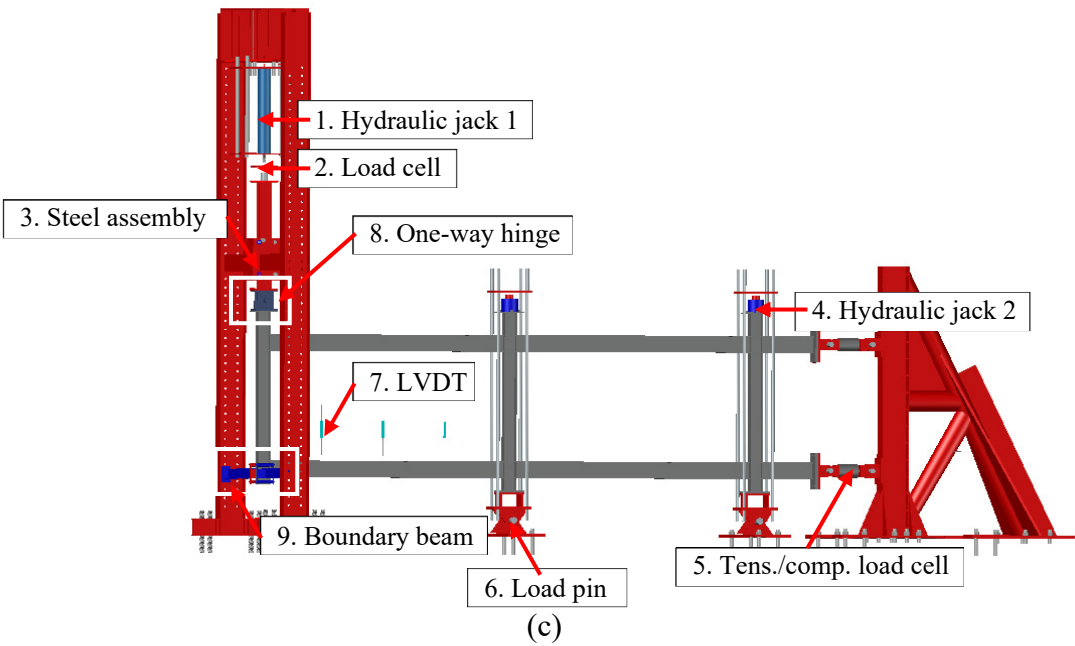
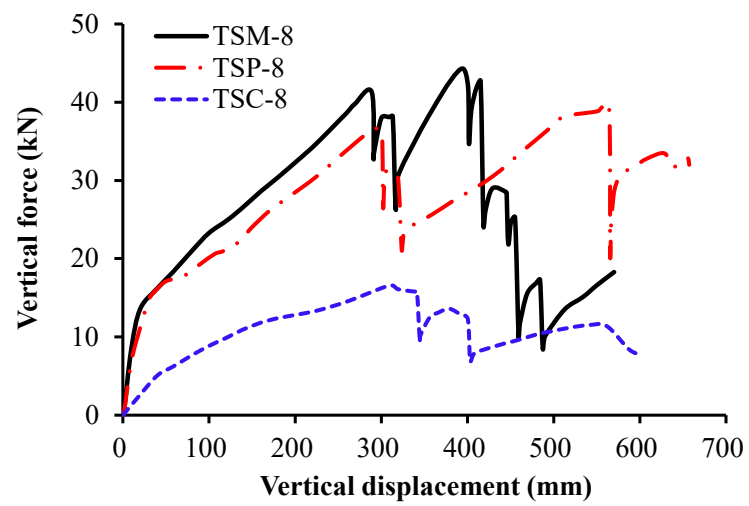
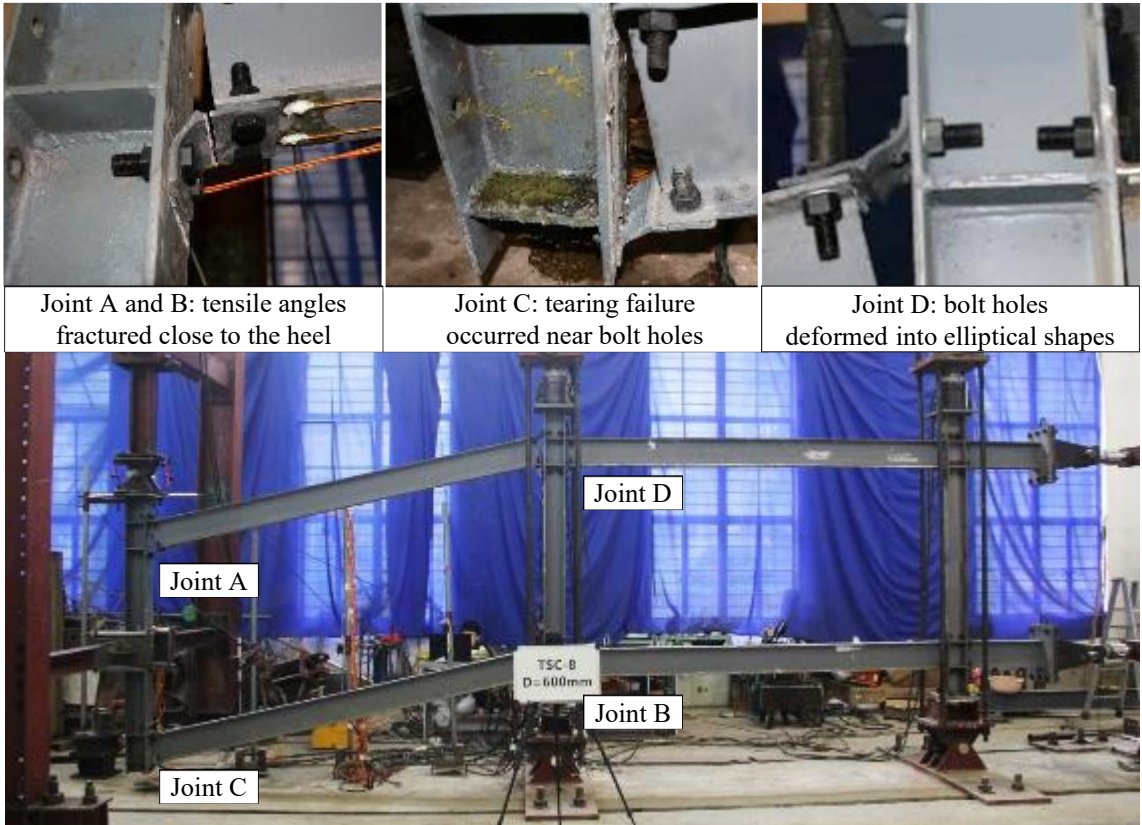
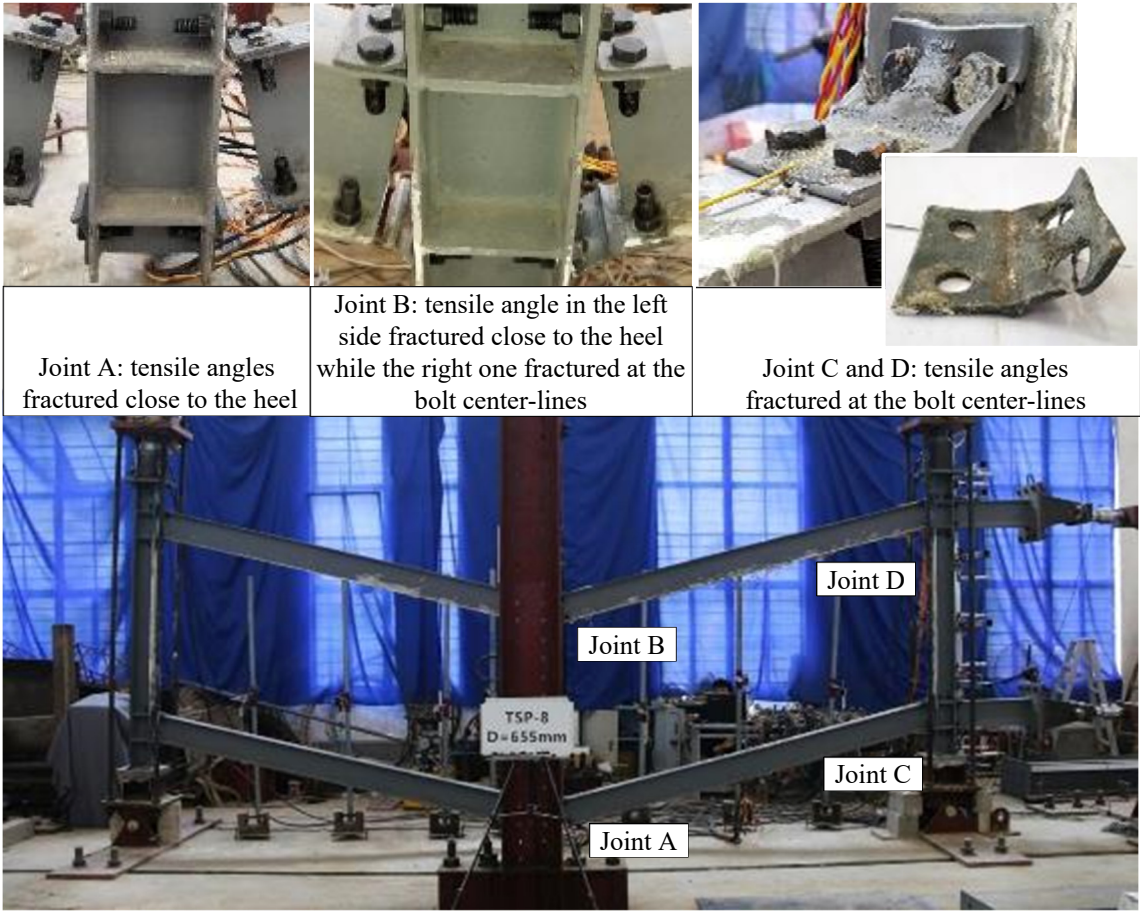


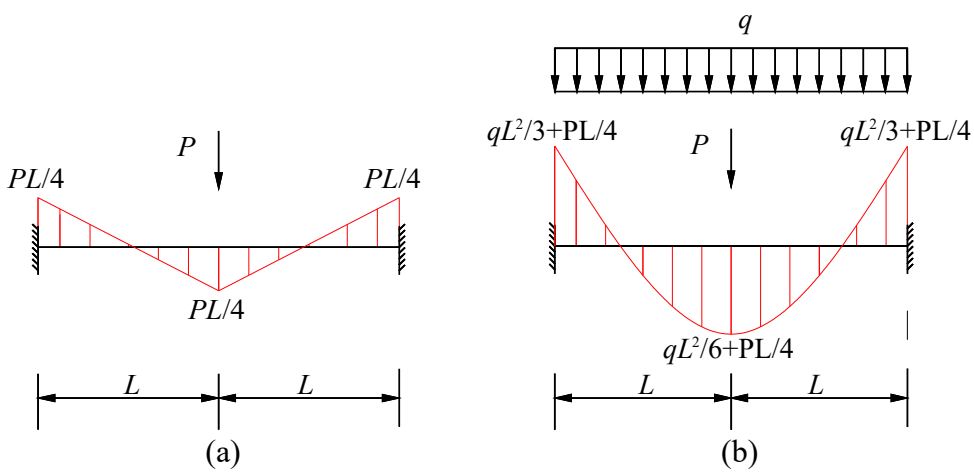
Figure 5

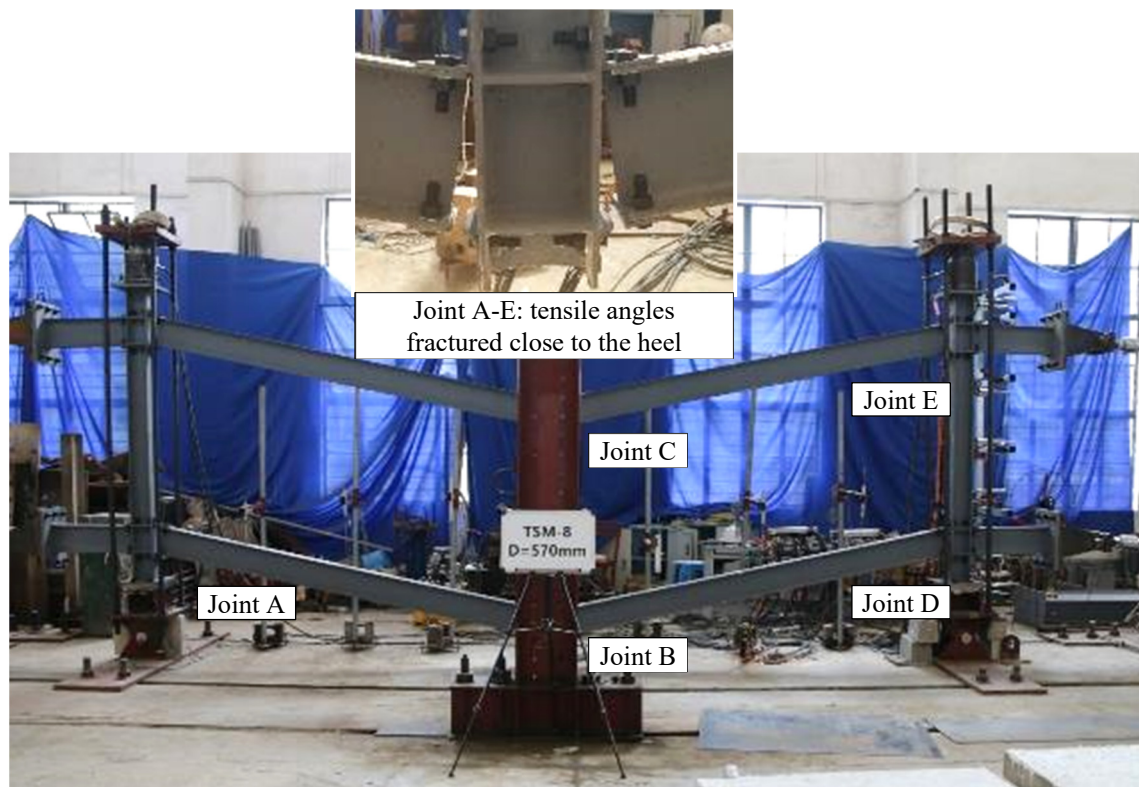


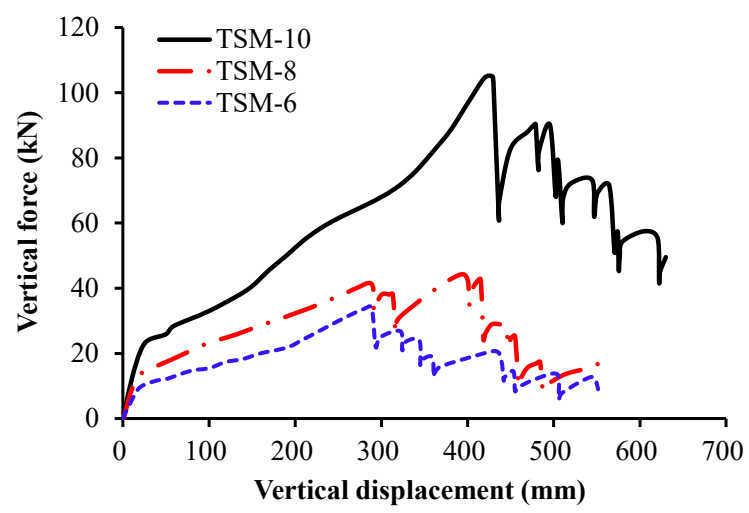


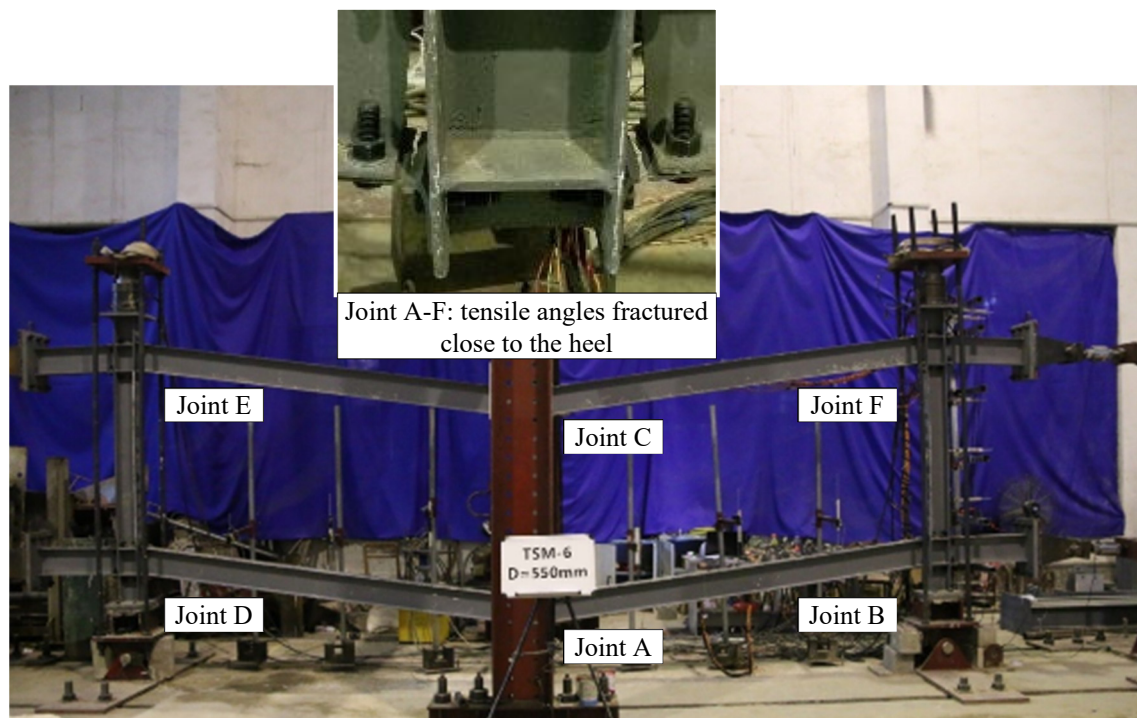


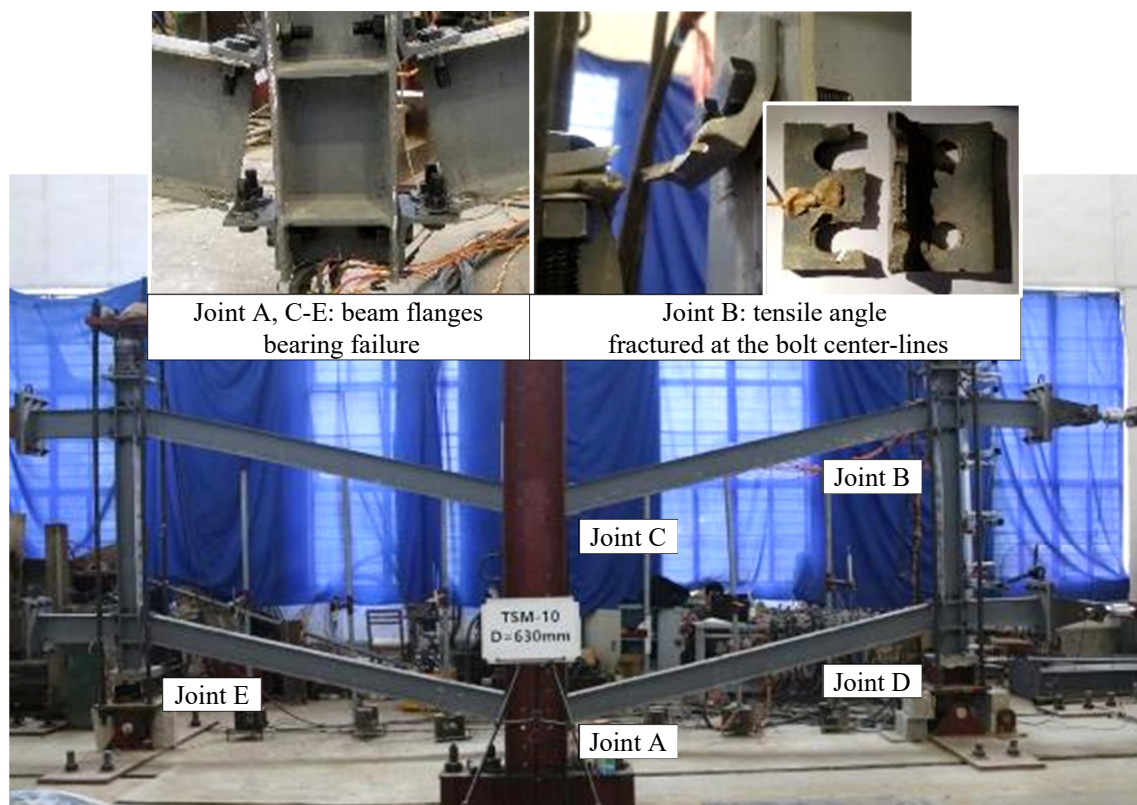
1

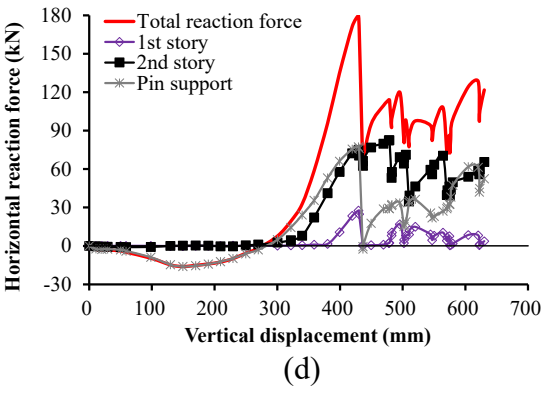
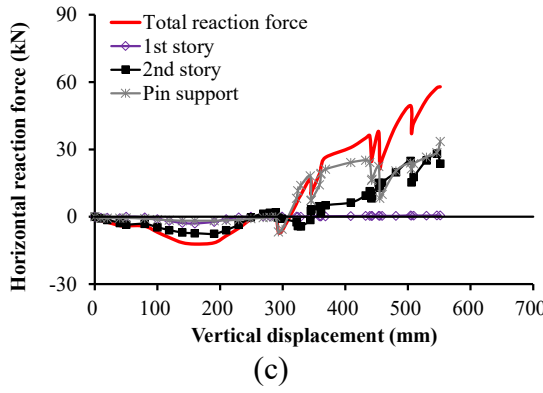
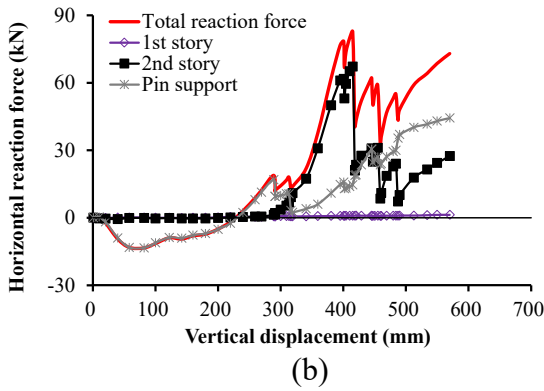
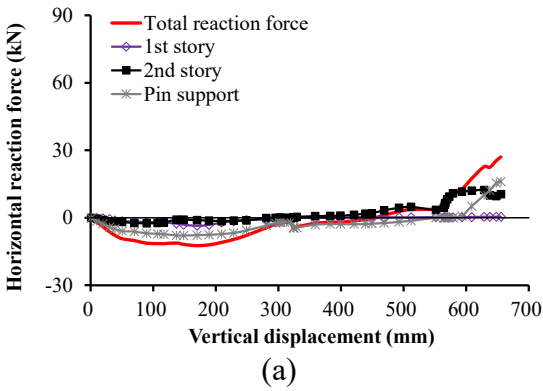


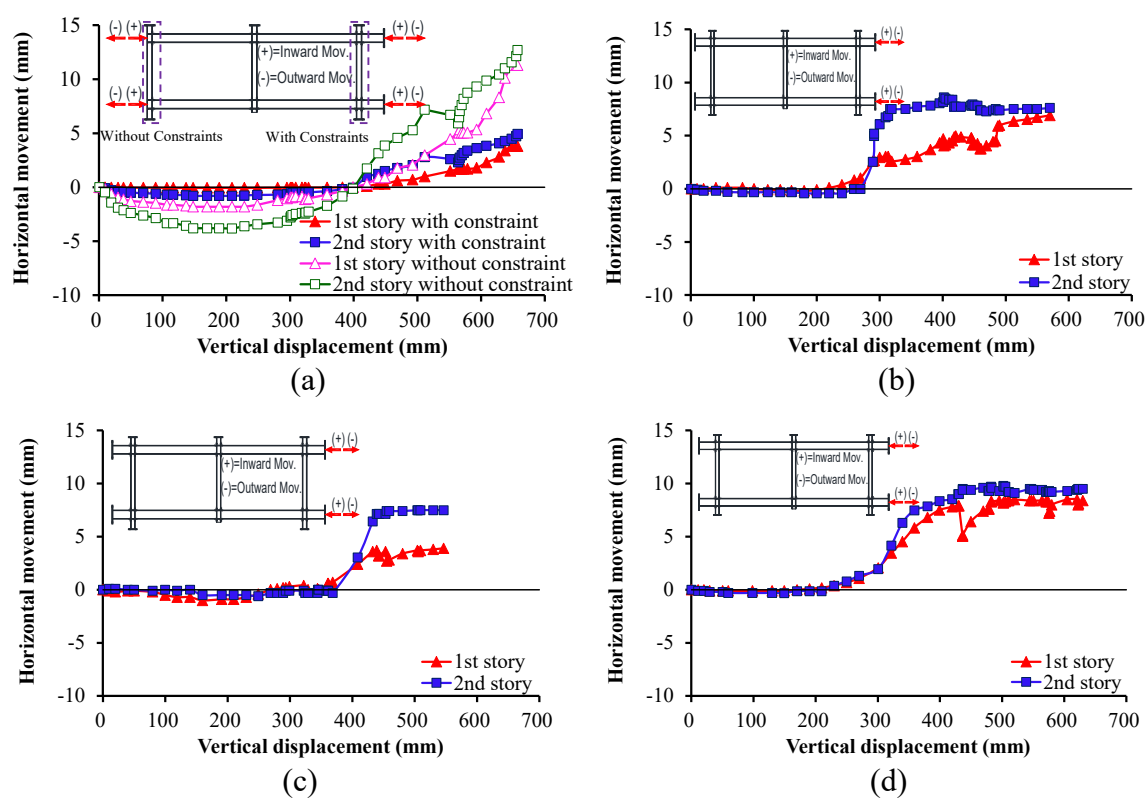


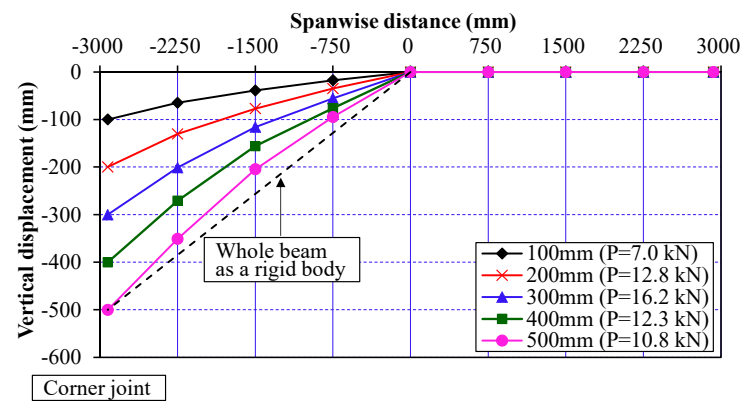




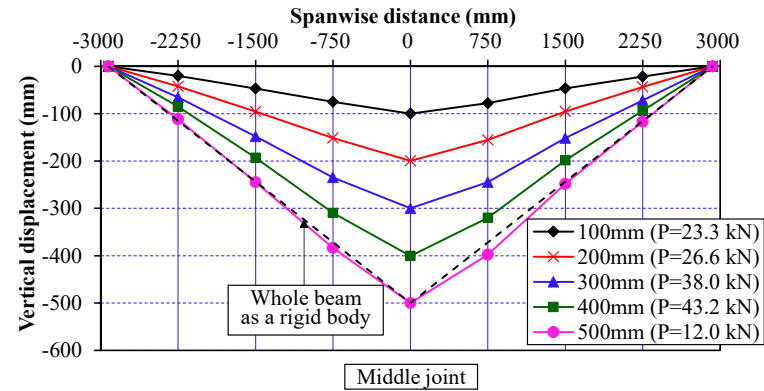




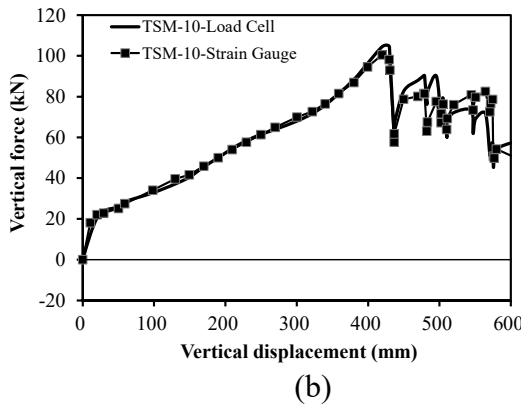
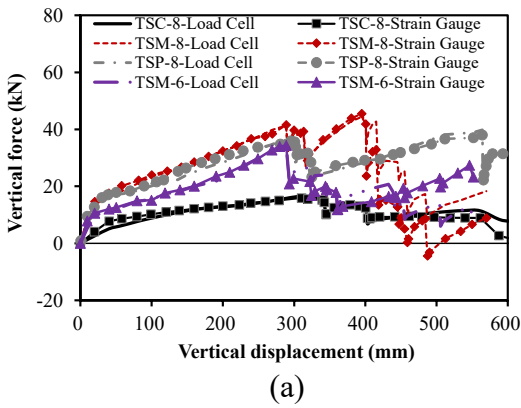




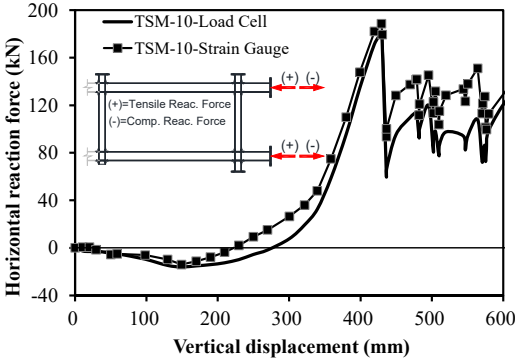
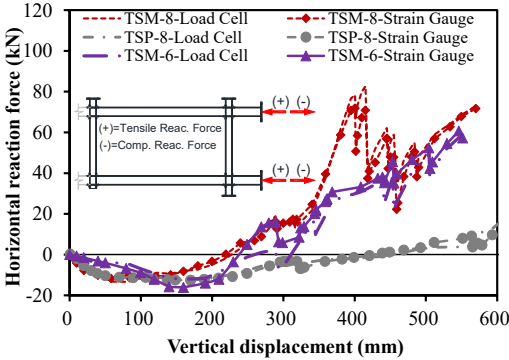
(a)

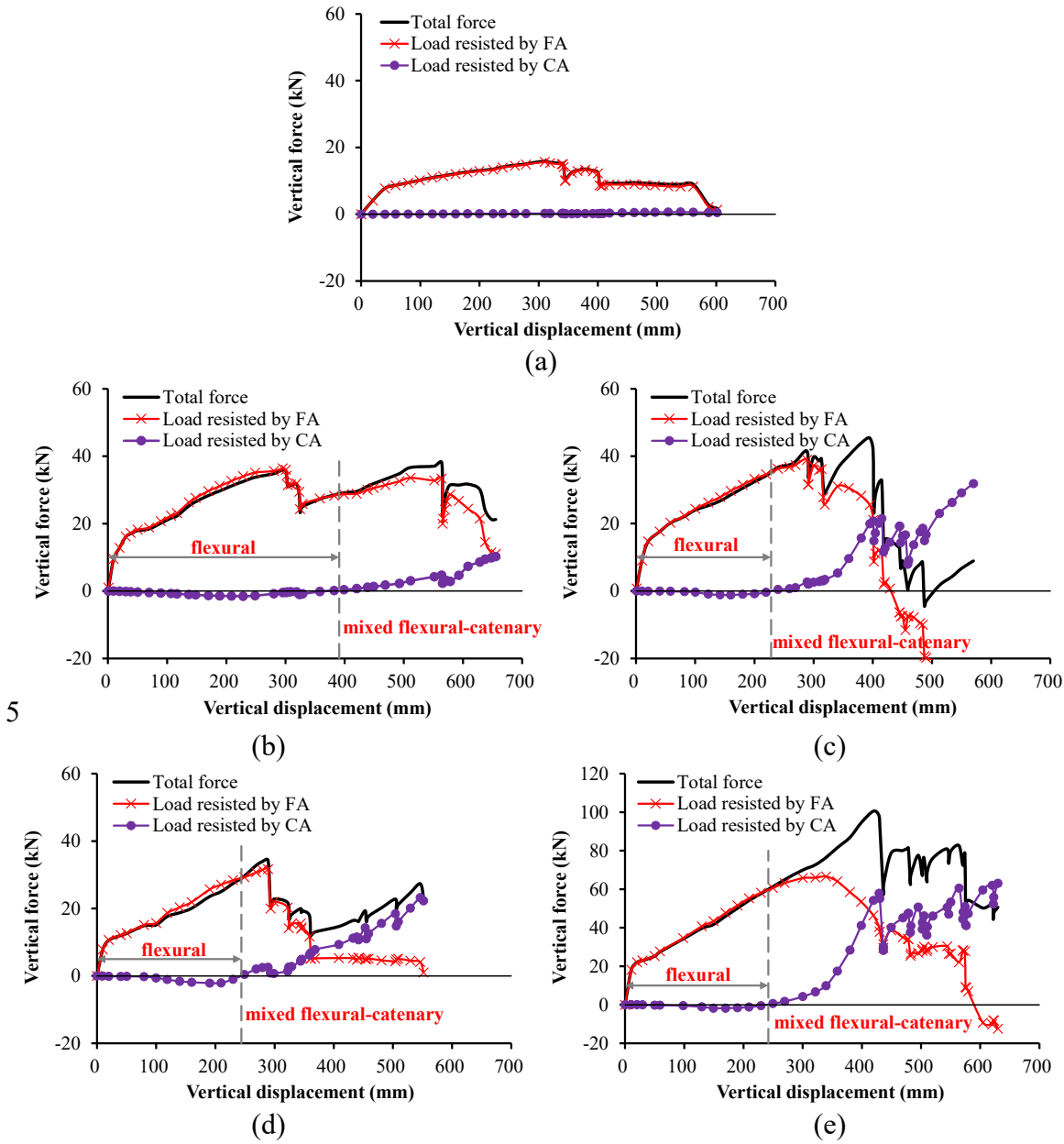


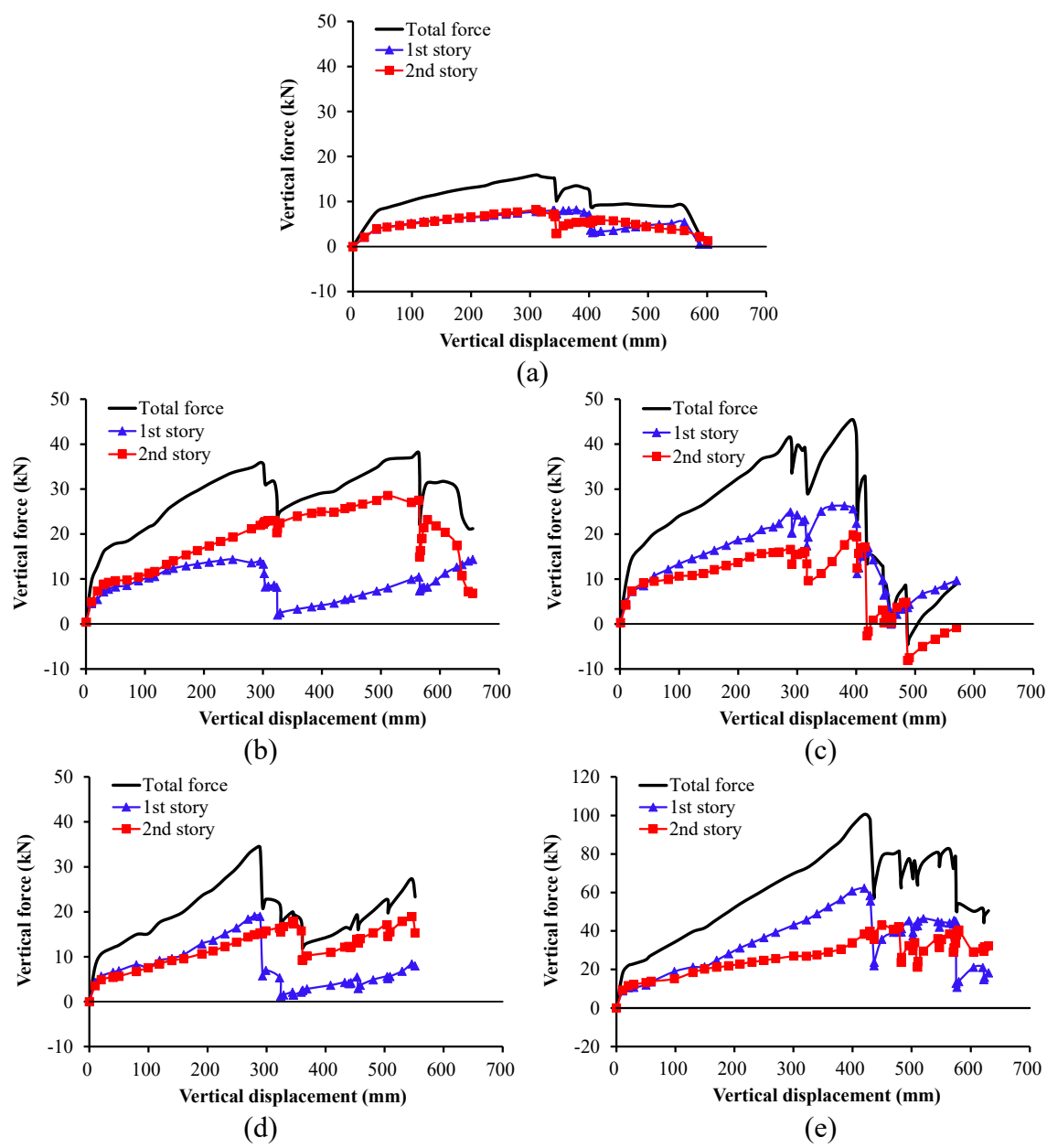
(b)

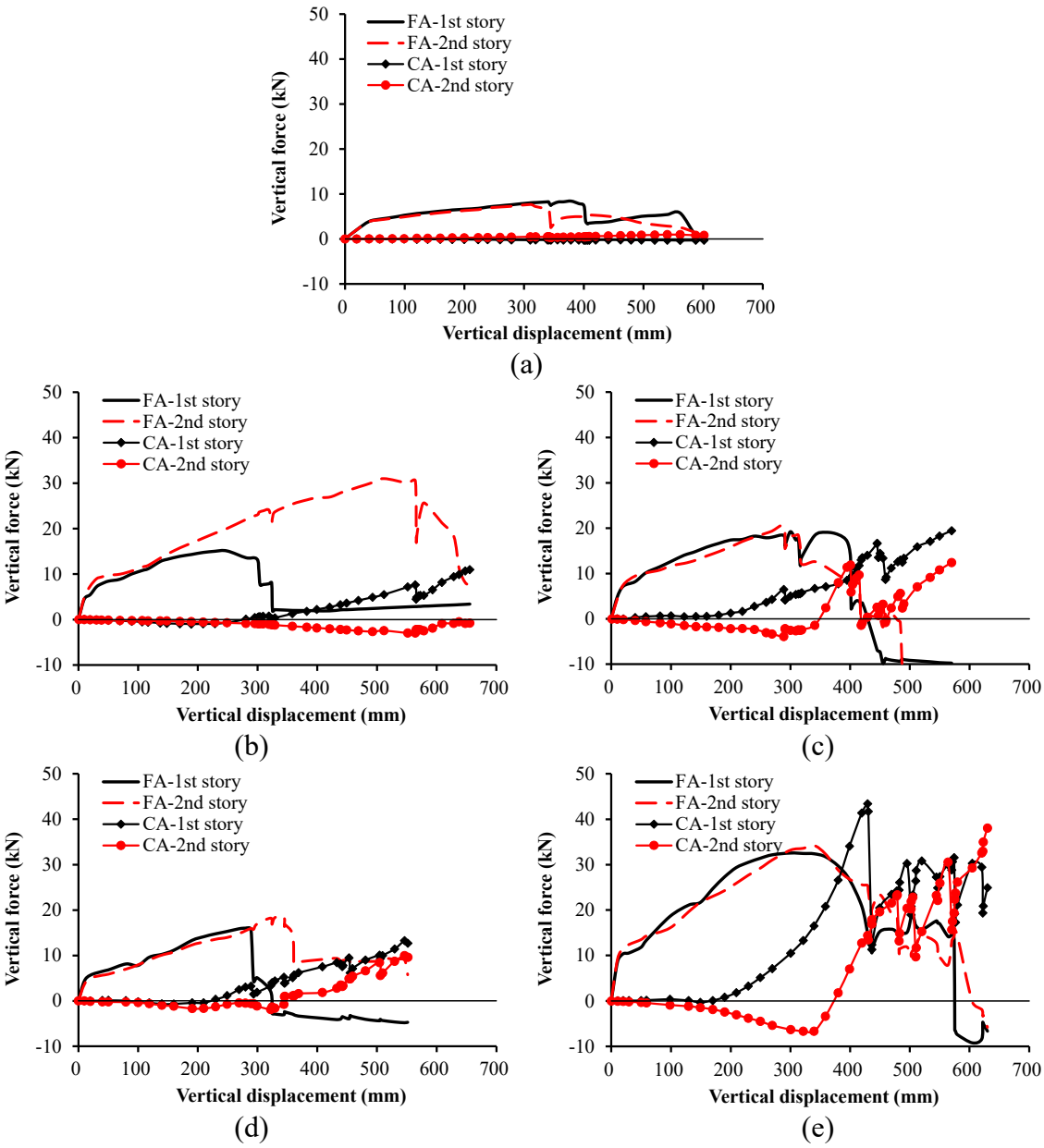


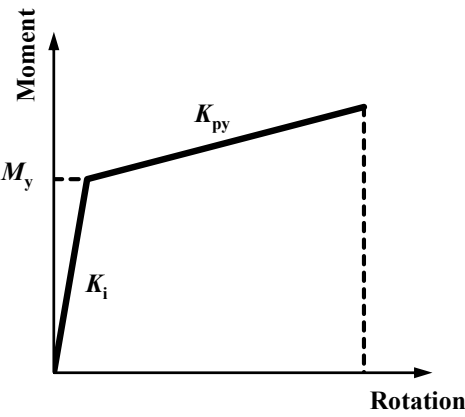
25
26
27
28
29
30
31
32
33
34
35
36
37
38
39
40
41
42
43

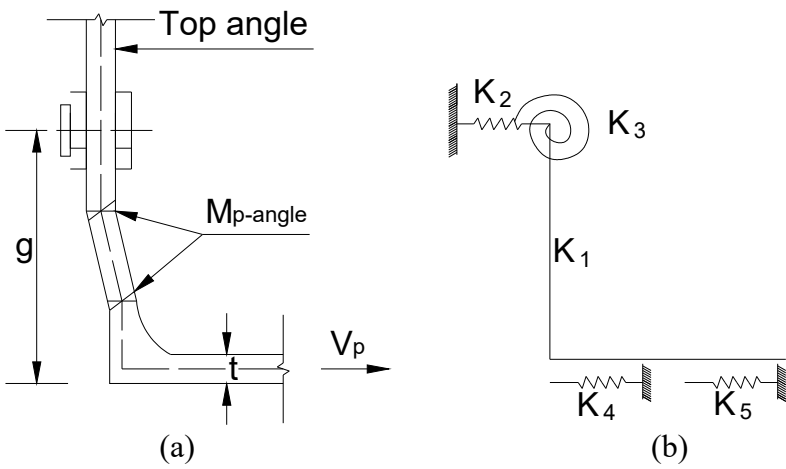


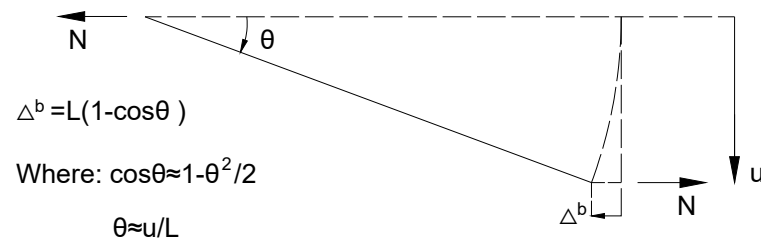




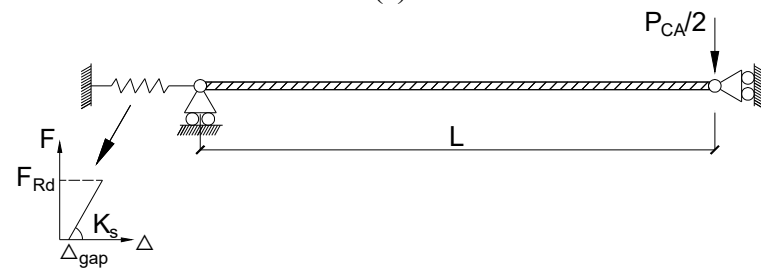








(a)



(b)

